

New approach to small transonic perturbations - Finite element numerical solving method - Part II: Numerical applications

J.-J. Angelini, Christian Soize

► **To cite this version:**

J.-J. Angelini, Christian Soize. New approach to small transonic perturbations - Finite element numerical solving method - Part II: Numerical applications. La Recherche Aérospatiale (English edition), 1989, 2 (-), pp.21-41. hal-00770320

HAL Id: hal-00770320

<https://hal-upec-upem.archives-ouvertes.fr/hal-00770320>

Submitted on 6 Mar 2021

HAL is a multi-disciplinary open access archive for the deposit and dissemination of scientific research documents, whether they are published or not. The documents may come from teaching and research institutions in France or abroad, or from public or private research centers.

L'archive ouverte pluridisciplinaire **HAL**, est destinée au dépôt et à la diffusion de documents scientifiques de niveau recherche, publiés ou non, émanant des établissements d'enseignement et de recherche français ou étrangers, des laboratoires publics ou privés.

NEW APPROACH .
TO SMALL TRANSONIC PERTURBATIONS
FINITE ELEMENT
NUMERICAL SOLVING METHOD

PART II: NUMERICAL APPLICATIONS

by

J. J. ANGELINI(*) and C. SOIZE(*)

ABSTRACT

In this Part II, we give some numerical applications of the finite element numerical solving method exposed in part I, for the unsteady small transonic perturbation. A 2-D code has been developed to validate the proposed approach. We present some numerical results for airfoils. Steady and unsteady transonic flows are mainly considered. These results are a validation of the Part I developments.

Keywords (NASA thesaurus): Aerodynamics — Transonic flow — Numerical methods — Finite element method.

(*) ONERA, B.P. 72, 92322 Châtillon Cedex.

II. — NUMERICAL APPLICATIONS

II.1. — INTRODUCTION

In Part I, we described a time-implicit finite element numerical solving method with mixed variables: physical/entropic variables, for unsteady conservative non-linear hyperbolic systems. This method can be applied in particular to the Euler equations.

We then showed that this formalism could be applied to the 3D unsteady small transonic perturbation equations. We obtained a new form of the small transonic perturbation equations in physical variables, which have rotational solutions and which allow body interactions to be accounted for, contrary to the potential small transonic perturbation equations in ADI scheme on structured meshes.

In Part II, we give numerical results for 2D transonic steady and unsteady flows which validate the numerical method proposed, in the framework of approximation of small transonic perturbations. This 2D code was also developed to verify the feasibility of development of an isentropic unsteady transonic 3D code in an unstructured mesh. Finally, the equations and the solving method chosen supply a code which operates in direct mode and inverse mode as well as in linear mode (subsonic and supersonic).

II.2. — DEVELOPMENT OF THE 2D PROGRAM

We developed a 2D code based on the equations of Sections 4,4 to 4,8 of Part I.

II.2.1. — CONSTANTS OF THE SCHEME

The only constants of the scheme are μ_0 and μ_1 , introduced in equation (I-73). They were numerically calibrated. We obtained:

$$\mu_0 = 0.45, \quad \mu_1 = 0.6.$$

These constants are independent of the problem treated, *i.e.* of the mesh, the time step, the Mach number, the angle of attack, etc. These fixed values are used for all the numerical applications given in Sections II,3 and II,4.

II.2.2. — CONVERGENCE NORM FOR THE STEADY CASE

In addition to the lift and moment on the airfoils, we use the criterion $\log(R2)$ for the field, where $R2$ is the following norm:

$$R2 = \left[|\Omega|^{-1} \sum_{J=1}^{M_v} CS_J \{K(\Delta t)^{-1} (W_1^{n+1} - W_1^n)_J\}^2 \right]^{1/2}$$

where CS_J is the area of the finite volume element (cell) J , M_v is the number of cells, $|\Omega| = \sum_{J=1}^{M_v} CS_J$ is the measure of domain Ω and W_1 is the first component (ρ) of W .

For the steady case, the tolerance on convergence of the conjugate gradient is controlled with respect to $\log(R2)$.

II.2.3. — U AND W REPRESENTATION

As functions U of the approximation space \mathcal{U} have a trace on the boundaries, the pressure coefficients C_p , the local Mach numbers, etc. are naturally calculated with U . Equation (I-12) must be verified numerically, *i.e.* $U = \nabla_W S(W) = \tilde{H}(W)W$. In the field, we take the norm L^2 of field $U - \nabla_W S(W)$, written on each finite volume element $\cup - \tilde{H}(W)W$, where \cup is the barycenter of the values of U at the apex nodes of the element and W is the constant value of W on the same element.

We also computed the pressure coefficients C_p , denoted CPR, in W representation. Since the functions W of \mathcal{W} do not have a trace on the boundaries, we used a local lifting. In each node I of an airfoil boundary, the lifting value of W in this node, denoted WR , was computed by:

$$WR = (\sum_J CS_J)^{-1} \sum_J CS_J W^{(J)}$$

extending the summing to all the finite volume elements J which have a common apex with node I , where $W^{(J)}$ is the value of W on each of elements J . The lifting chosen is only an approximation which is also the case for the lifting pressure coefficient CPR. However, except for the lifting approximation, the comparison of C_p (in U representation) with CPR (in lifted W representation) gives a very good indication of equation (I-12) from a numerical standpoint.

II.2.4. — COMPUTATION OF THE CFL FOR THE STEADY CASE

In the method developed, the time step Δt is not local for the steady case. For each finite volume element $J \in \{1, \dots, M_v\}$, the local time step, denoted Δt_J , is defined by $\Delta t_J = L_J/V_J$, where:

$$L_J = (CS_J)^{1/2}, \quad V_J = 1 + M^{-1} (1 - \lambda W_2^{(J)})^{1/2}.$$

Under the usual conditions of functioning of an explicit scheme, a time step Δt should be taken, then denoted Δt_{expl} , such that:

$$\Delta t_{\text{expl}} \simeq \min_{J \in \{1, \dots, M_v\}} \{\Delta t_J\}.$$

If Δt is the time step, considered fixed, of the present implicit scheme, we then define the CFL by $\text{CFL} = \Delta t / \Delta t_{\text{expl}}$, *i. e.*:

$$\text{CFL} = \max_{J \in \{1, \dots, M_v\}} \{\Delta t / \Delta t_J\}.$$

II.3. — NUMERICAL CASES TREATED

II.3.1. — STEADY COMPUTATIONS

Below we give the results of the steady computations for the following cases:

C1S: NACA12 airfoil, Mach 0.8, angle of attack 0 degrees.

C2S: NACA12 airfoil, Mach 0.85, angle of attack 1 degree.

C3S: NACA12 airfoil, Mach 0.15, angle of attack 0 degrees.

C4S: Biplane NACA12 airfoils, Mach 0.58, angle of attack 0 degrees.

C5S: Biplane NACA12 airfoils, Mach 0.58, angle of attack 6 degrees.

C6S: S airfoil, Mach 0.735, angle of attack 0.6 degrees.

(1) For C4S and C5S, the Mach number used, 0.58, is different from the reference Mach number which is 0.55. We will explain why.

(2) The S airfoil of the C6S case is the profile of a supercritical wing section of a transport aircraft of

the Airbus family. The influence of the mesh is discussed for this airfoil. Three meshes are considered.

(3) For all the steady computations, the initialization is the zero uniform field (the variables of the formulation are perturbation variables).

(4) The computation time step Δt is the same for all the steady results given. As the period is 2π , we took $\Delta t = 2\pi/N_S$ with $N_S = 256$ and $K_S = 1$ as reduced frequency. Thus, for all the steady computations, we have:

$$(K/\Delta t)_S = (2\pi)^{-1} K_S N_S = 256/(2\pi).$$

II.3.2. — UNSTEADY COMPUTATIONS

The unsteady results given correspond to the following cases:

C1INS: NACA12 airfoil, Mach 0.85, steady angle of attack 1 degree.

C2INS: NACA12 airfoil, Mach 0.8, steady angle of attack 0 degrees.

C3INS: S airfoil, Mach 0.735, steady angle of attack 0.6 degrees.

(1) For all the unsteady computations, the movement is a forward quarter pitch with an amplitude of 1 degree around the steady angle of attack.

(2) The initialization of each unsteady computation is the associated steady solution, *i. e.* C2S for C1INS, C1S for C2INS and C6S for C3INS.

(3) For each unsteady computation, the time step Δt was chosen such that:

$$(K/\Delta t)_{\text{INS}} = (K/\Delta t)_S.$$

Denoting the number of time steps per period as N_{INS} , we have $\Delta t_{\text{INS}} = 2\pi/N_{\text{INS}}$, and:

$$N_{\text{INS}} = K_S N_S / K_{\text{INS}} = 256 / K_{\text{INS}}.$$

Thus, for a reduced frequency $K_{\text{INS}} = 2$ (or $K_{\text{INS}} = 0.25$), we have $N_{\text{INS}} = 128$ (or $N_{\text{INS}} = 1024$).

II.3.3. — THE MESHES

Five meshes are used. The characteristics and use of the meshes are given in Table I.

TABLE I
Meshes used.

| Airfoil | Number of cells | Number of points on the airfoil | Figure | Use in the: | |
|-----------|-----------------|---------------------------------|---------|---------------|---------------|
| | | | | Steady case | Unsteady case |
| NACA12 | 9.338 | 196 | 1 and 2 | CS1, CS2, CS3 | C1INS, C2INS |
| BI-NACA12 | 12.280 | 2 × 154 | 11, 12 | C4S, C5S | - |
| S | Mesh 1 | 5.502 | 100 | C6S | C3INS |
| | Mesh 2 | 6.628 | 174 | | |
| | Mesh 3 | 7.254 | 154 | | |

For the S airfoil, the three meshes (Figs. 15, 16, 19, 22) differ only in the proximal region of the airfoil. Meshes 1 and 2 differ by the number of points on the airfoil. Mesh 3 is similar to mesh 2 on the airfoil with a higher concentration in the leading edge region. This mesh, which contains very small mesh cells, was introduced to illustrate the robustness of the numerical method.

II.4. — NUMERICAL RESULTS

II.4.1. — STEADY COMPUTATIONS

On all the steady pressure coefficient figures, the ordinate is $-C_p$ and the abscissa is $x_1 = X_1/C \in [0, 1]$. Both the upper and lower surface are shown together in each figure (Figs. 3-6, 8, 10, 13, 14, 17, 20, 23).

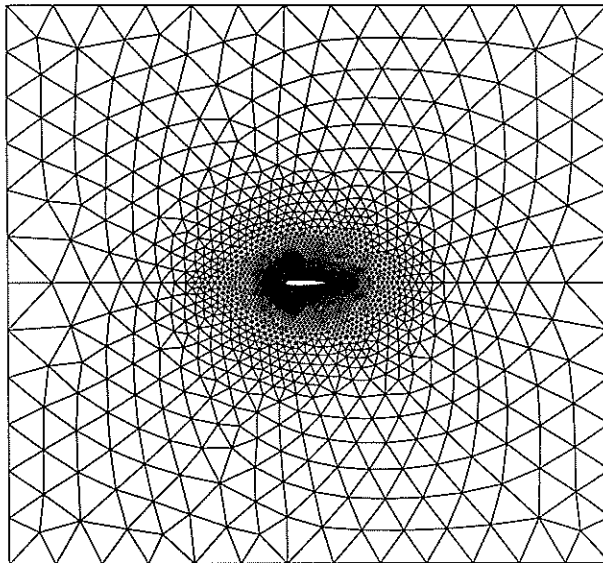


Fig. 1. — Complete view of the mesh of the computation domain. NACA12 airfoil.

The steady pressure coefficients given correspond to the convergence state indicated by graphs $n \mapsto \log(R2(n))$, where n is the number of the time step (Figs. 7, 9, 18, 21, 24). In Figures 7 and 9, it can be seen that the norm increases locally, due to the dynamics of the problem (shock displacement), whereas the dynamics are preserved in the steady computations (the computations are actually made for the unsteady case).

For all cases, we always verified that equation (I-12) was satisfied numerically (Sec. II.2.3). For obvious reasons of space, we did not give all the graphs and we restricted ourselves, to illustrate this aspect, to case C1S. Figure 3, showing the U and W

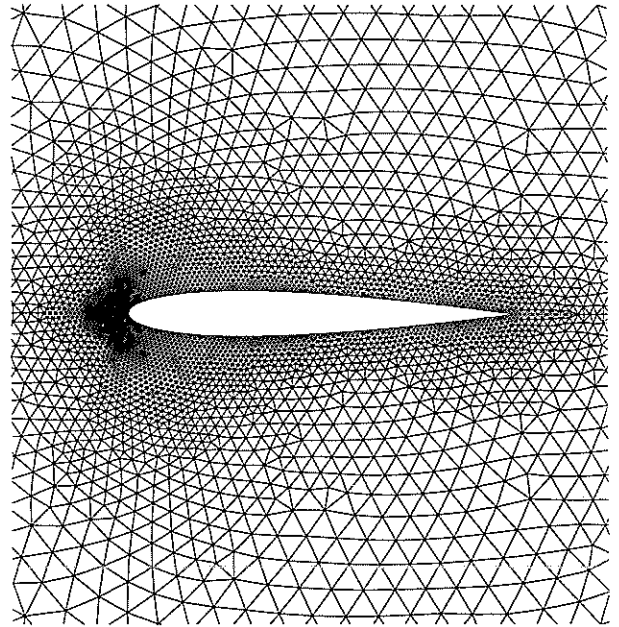


Fig. 2. — Partial view of the mesh of the computation domain. NACA12 airfoil.

representations of $-C_p$ superimposed, demonstrate that the equation is effectively satisfied.

C1S Results: These results are illustrated in Figures 3 to 7. Figure 6 shows the steady pressure coefficient on the airfoil, obtained with the potential 2D small transonic perturbation code in ADI scheme on a structured mesh. The comparison of Figure 6 with Figures 4 and 5 shows that practically the same solution is obtained. At convergence, we have $CFL=18$ and the lower and upper surface shock is located at $x_1=0.498$.

C2S Results: Figure 8 shows the steady pressure coefficient $-C_p$ on the upper surface and lower surface. The flow exhibits two relatively strong shocks. At convergence, we have $CFL=18$ and Table II gives the position of the shocks, the drag, the lift and the moment, compared with W. Schmidt and A. Jameson's reference solution (taken from [1]), constructed with the Euler equations.

TABLE II
NACA12, Mach 0.85, Angle of attack 1 degree.

| | Results | Reference solution |
|---------------------|---------|--------------------|
| Lower surface shock | 0.6230 | 0.6458 |
| Upper surface shock | 0.8750 | 0.8624 |
| Drag | 0.0733 | 0.0580 |
| Lift | 0.3510 | 0.3584 |
| Moment | 0.1232 | 0.1228 |

These results show that the small transonic perturbation equations considered give a very good approximation of the Euler equations in this case.

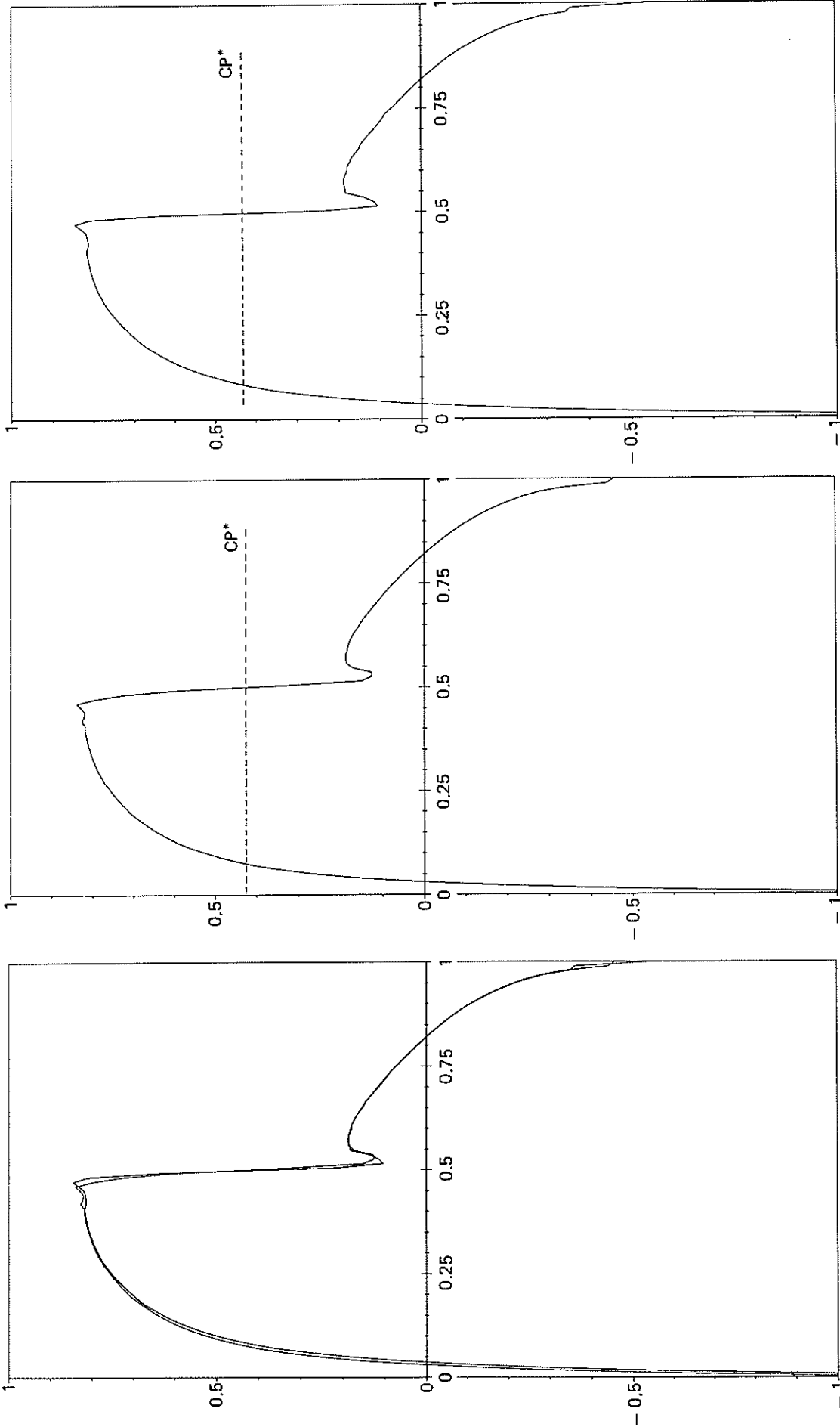


Fig. 5. — Steady pressure coefficient $-C_p$, upper surface and lower surface, in W representation. Mach 0.8, angle of attack 0 degrees, NACA12 airfoil.

Fig. 4. — Steady pressure coefficient $-C_p$, upper surface and lower surface, in U representation. Mach 0.8, angle of attack 0 degrees, NACA12 airfoil.

Fig. 3. — Steady pressure coefficient $-C_p$, upper surface and lower surface, in U and W representation. Mach 0.8, angle of attack 0 degrees, NACA12 airfoil.

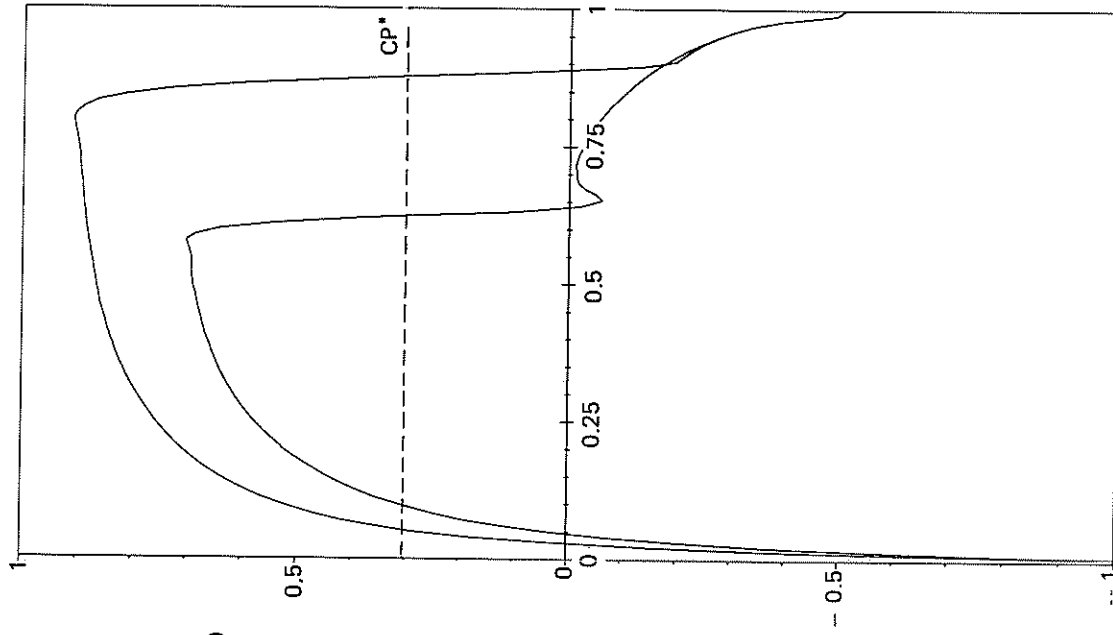


Fig. 8. — Steady pressure coefficient $-C_p$, upper surface and lower surface, Mach 0.85, angle of attack 1 degree, NACA12 airfoil.

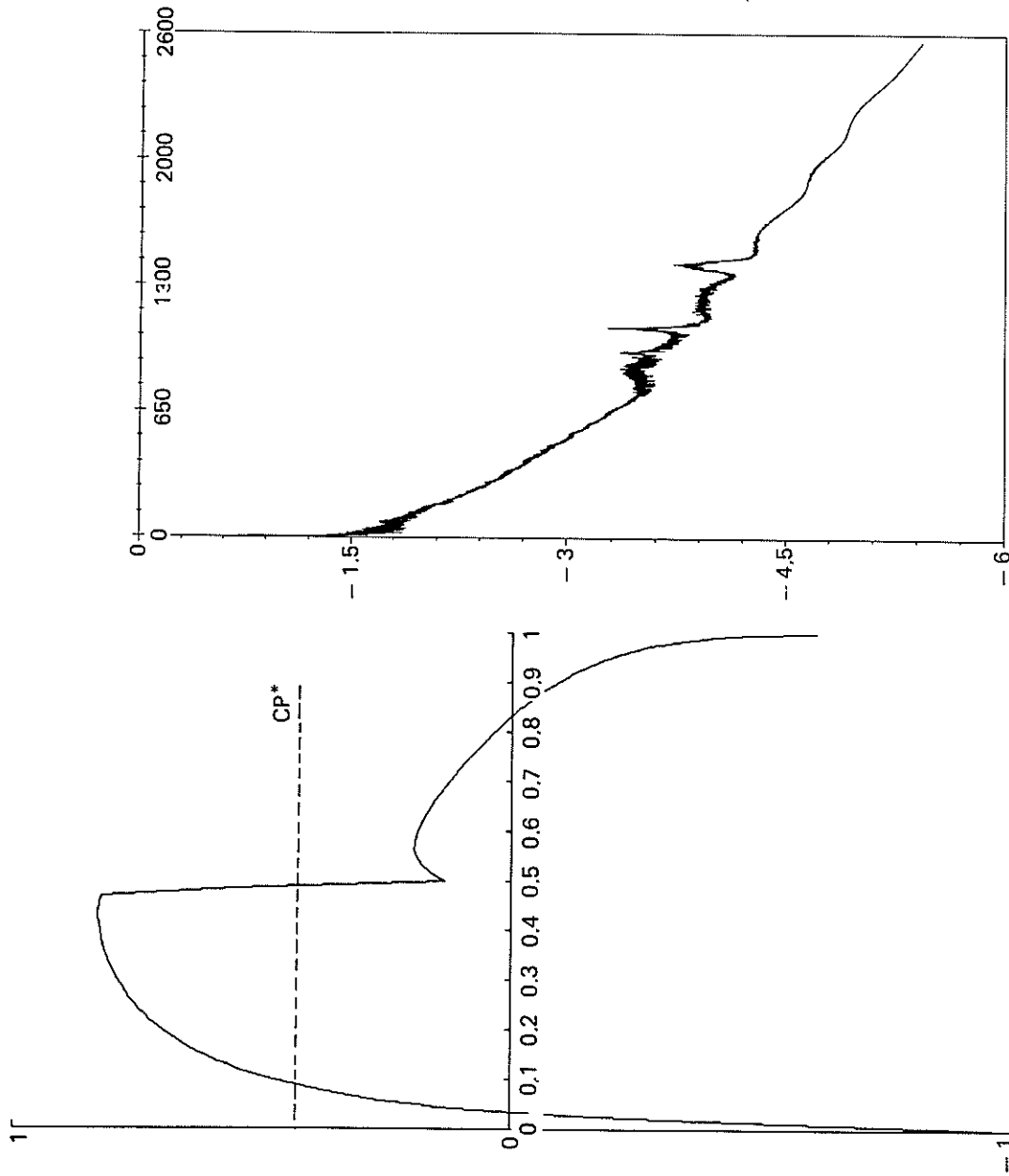


Fig. 7. — Steady convergence, $\log(R2)$, Mach 0.8, angle of attack 0 degrees, NACA12 airfoil.

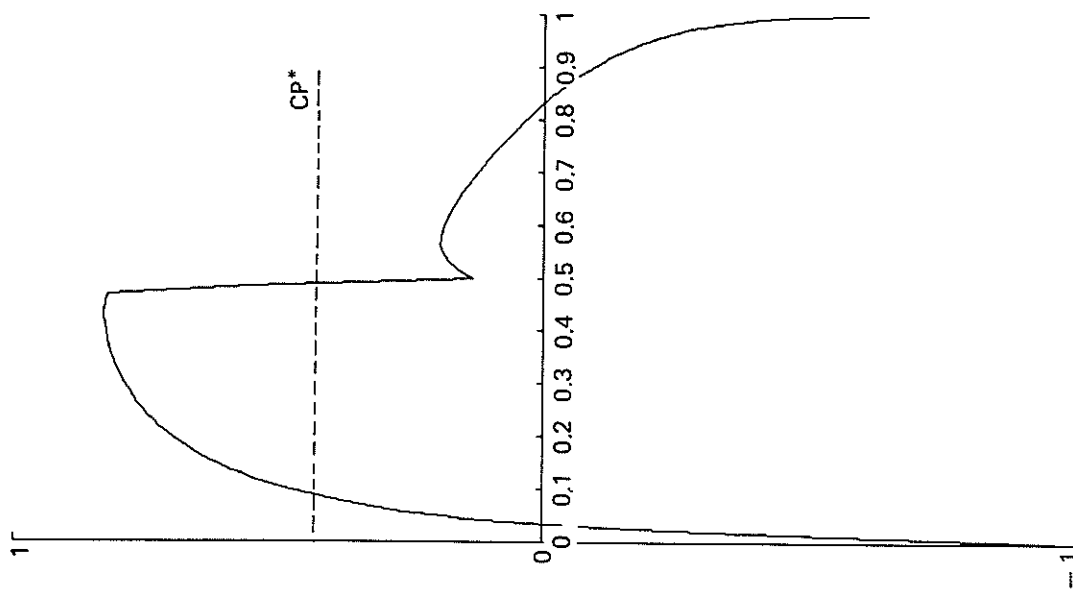


Fig. 6. — Steady pressure coefficient $-C_p$, upper surface and lower surface, obtained with the potential 2D small transonic perturbation code in ADI scheme on a structured mesh, Mach 0.8, angle of attack 0 degrees, NACA12 airfoil.

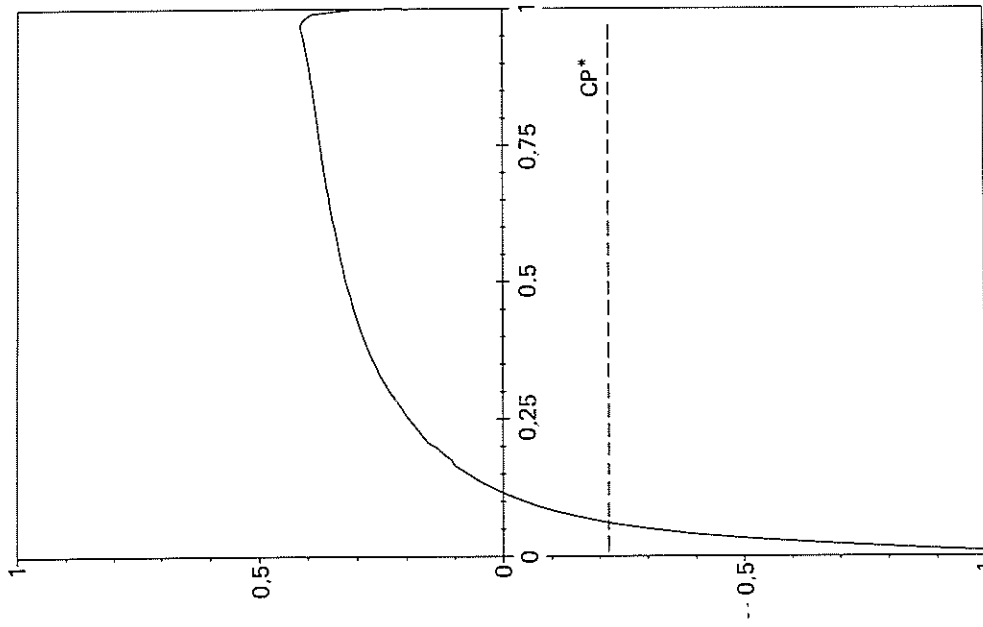


Fig. 10. — Mach 1.15, angle of attack 0 degrees.
Steady pressure coefficient $-C_p$, upper surface and lower surface.
NACA12 airfoil.

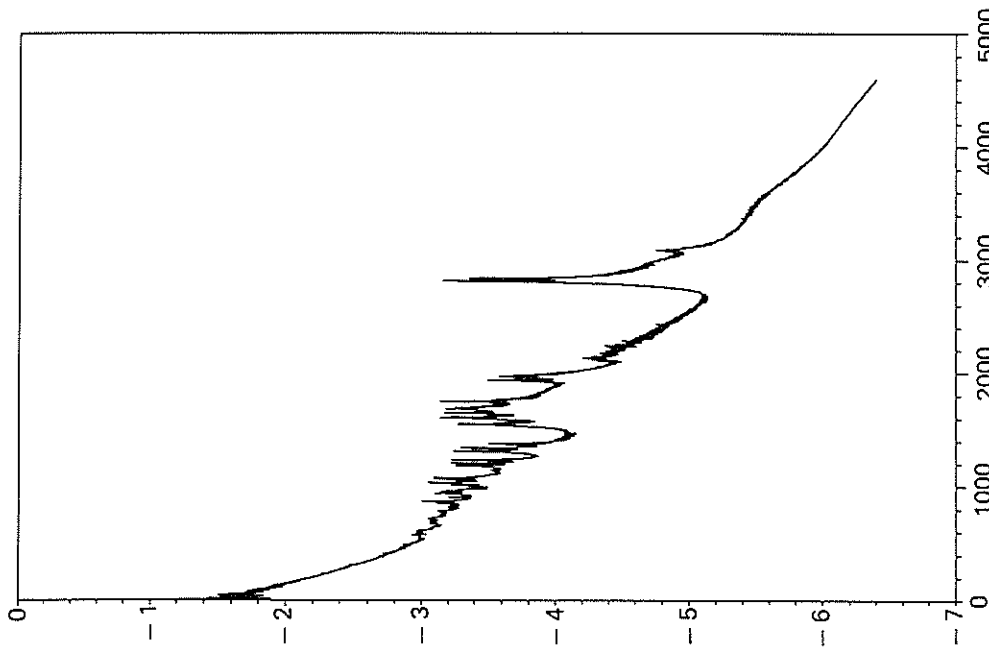


Fig. 9. — Steady convergence, $\log(R2)$.
Mach 0.85, angle of attack 1 degree,
NACA12 airfoil.

C3S Results: For this weakly supersonic case, Figure 10 shows the pressure coefficient of the airfoil. Here again, we obtain practically the same solution as with the Euler equations.

C4S and C5S Results: We made an initial computation at Mach 0.55 (reference case) for two angles of attack: 0 and 6 degrees. For this Mach number, we did not obtain a shock in the channel for 0 degrees or for 6 degrees. Figure 13 (and Figure 14) show the pressure coefficients $-C_p$ on the upper and lower airfoils for an angle of attack of 0 degrees (or 6 degrees) and a Mach number of 0.58. It is probable that this difficulty is due to the small transonic perturbation approximation and that, in this case, the critical Mach number is between 0.55 and 0.58. We can therefore not compare this result with the reference solution, constructed with the Euler equations, since the Mach number is not the same. In spite of this difference in Mach number, the solutions are close to one another [1, 2].

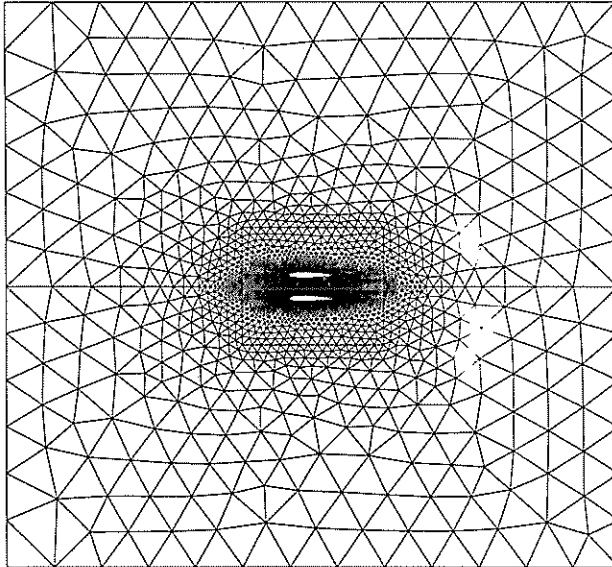


Fig. 11. — Complete view of the mesh of the computation domain.
Biplane NACA12 airfoil.

C6S Results: The results for the three meshes are given in Figures 17, 20 and 23. The values of the CFL and the overall values at convergence are summarized in Table III.

TABLE III

S airfoil, Mach 0.735, angle of attack 0.6 degrees.

| | Mesh 1 | Mesh 2 | Mesh 3 |
|--------|--------|--------|--------|
| CFL | 21 | 20 | 53 |
| Lift | 0.4663 | 0.4686 | 0.4759 |
| Moment | 0.1292 | 0.1277 | 0.1264 |

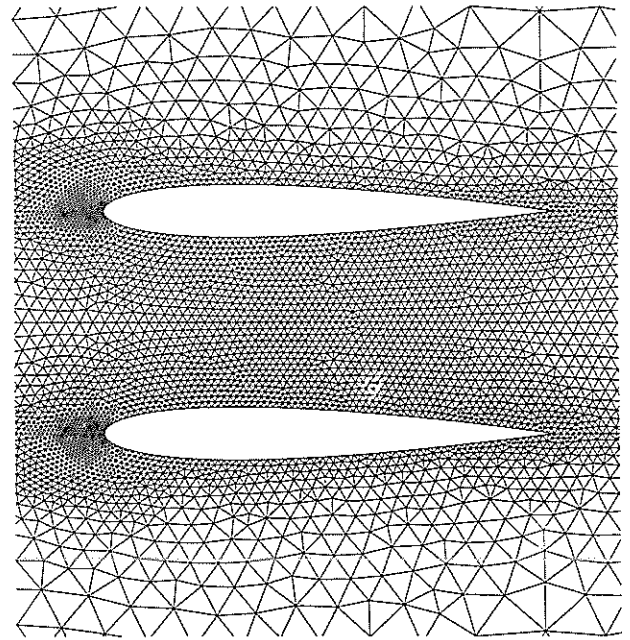


Fig. 12. — Partial view of the mesh of the computation domain.
Biplane NACA12 airfoil.

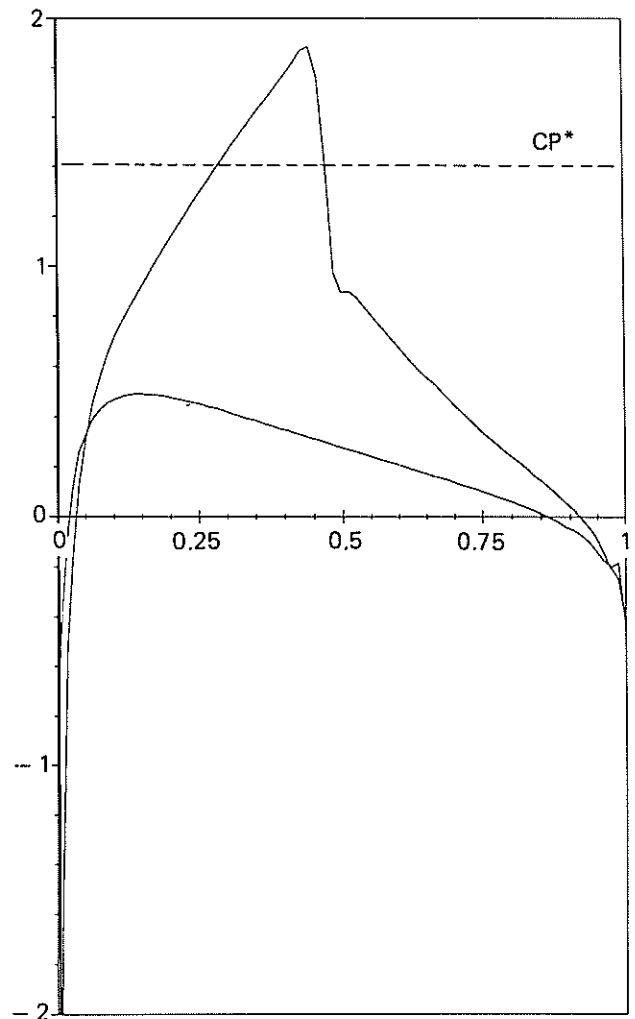


Fig. 13. — Mach 0.58, angle of attack 0 degrees, steady pressure coefficient $-C_p$, upper surface and lower surface on the upper and lower profiles, biplane NACA12 airfoil.

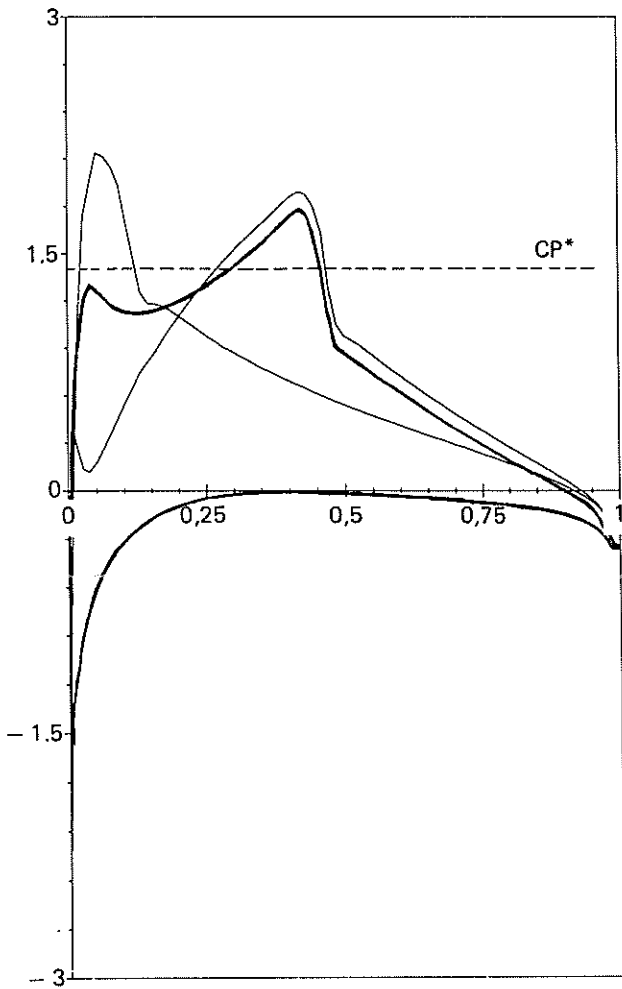


Fig. 14. — Mach 0.58, angle of attack 6 degrees, steady pressure coefficient $-C_p$, upper surface and lower surface of the upper profile, upper surface and lower surface of the lower profile. Biplane NACA12 airfoil.

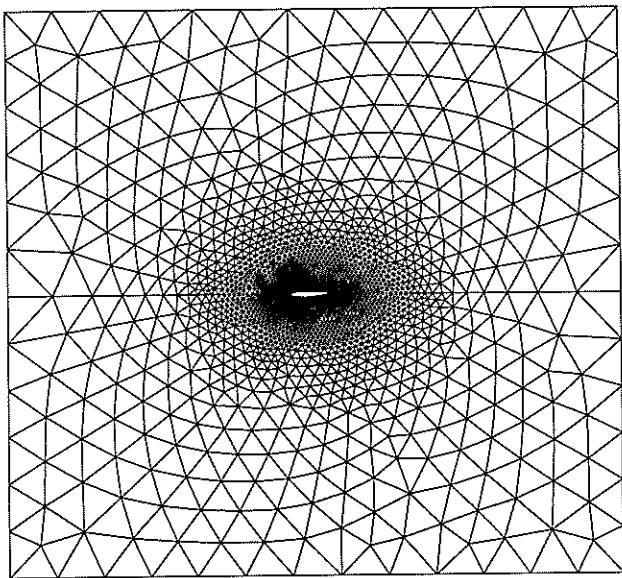


Fig. 15. — Complete view of mesh 1 of the computation domain. Supercritical S airfoil.

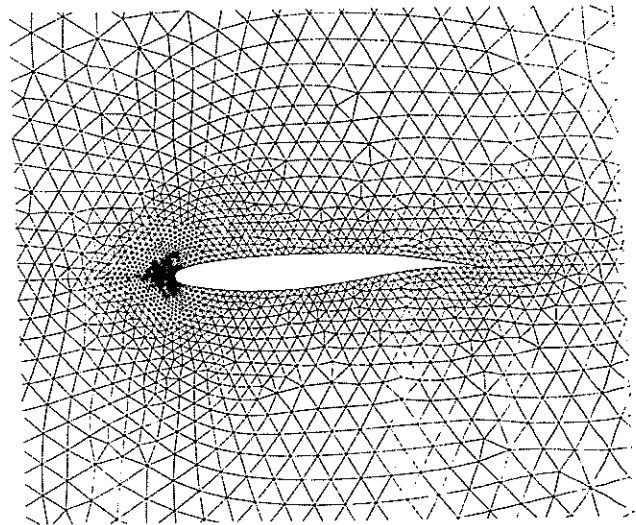


Fig. 16. — Partial view of mesh 1 of the computation domain. Supercritical S airfoil.

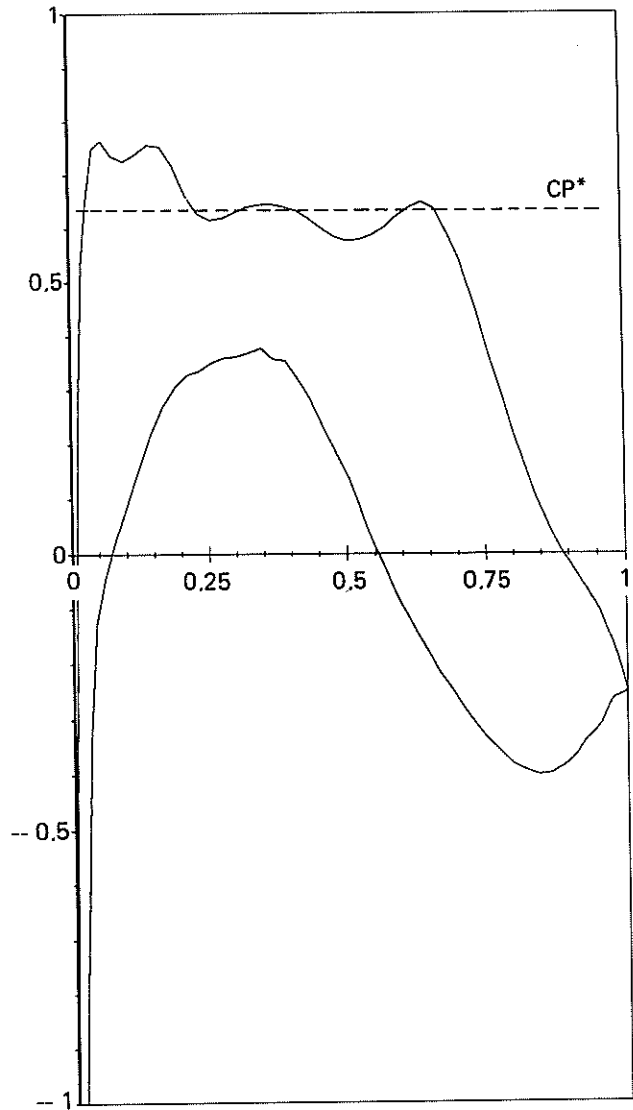


Fig. 17. — Steady pressure coefficient $-C_p$, upper surface and lower surface with mesh 1. Mach 0.735, angle of attack 0.6 degrees, Supercritical S airfoil.

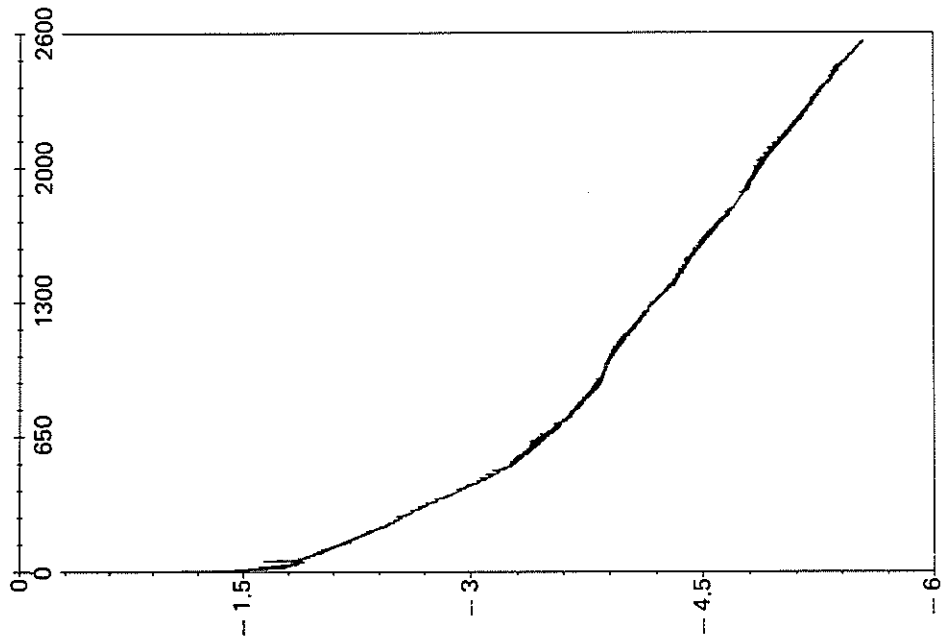


Fig. 18. — Steady convergence, $\log(R2)$, mesh 1. Mach 0.735, angle of attack 0.6 degrees. Supercritical S airfoil.

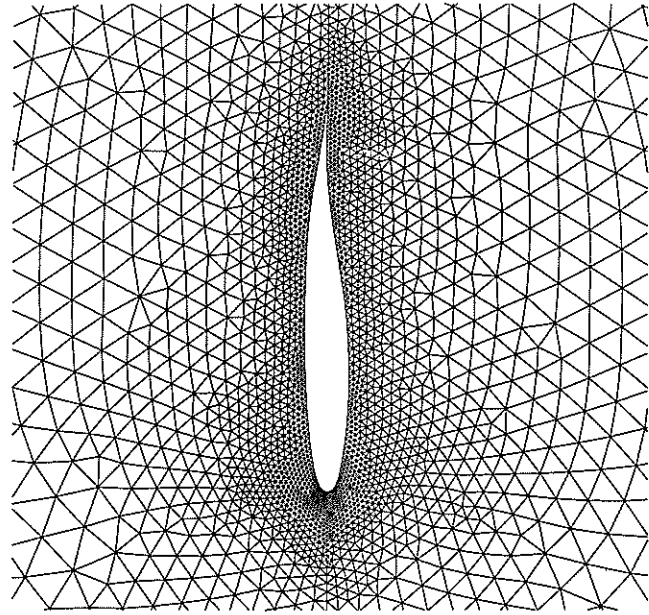


Fig. 19. — Partial view of mesh 2 of the computation domain. Supercritical S airfoil.

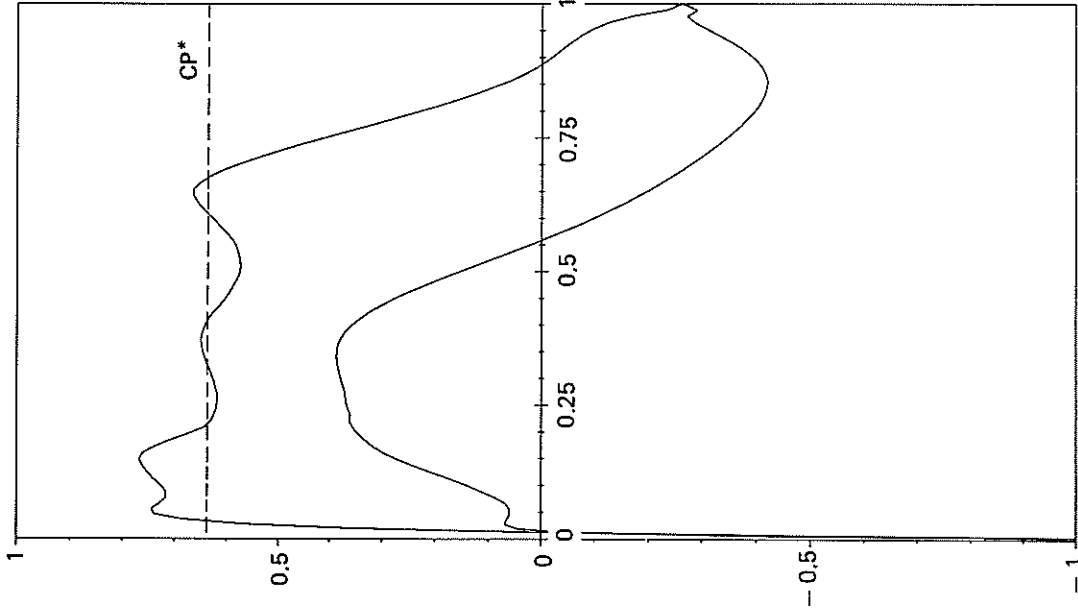


Fig. 20. — Steady pressure coefficient $-C_p'$, upper surface and lower surface with mesh 2. Mach 0.735, angle of attack 0.6 degrees, supercritical S airfoil.

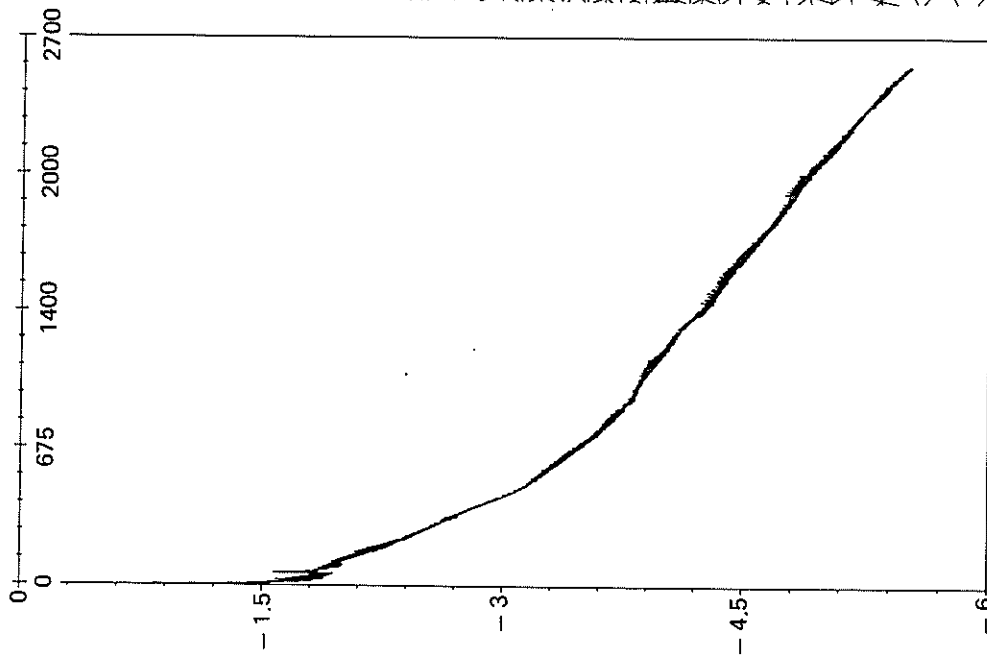


Fig. 21. — Steady convergence, log (R2), mesh 2. Mach 0.735, angle of attack 0.6 degrees, supercritical S airfoil.

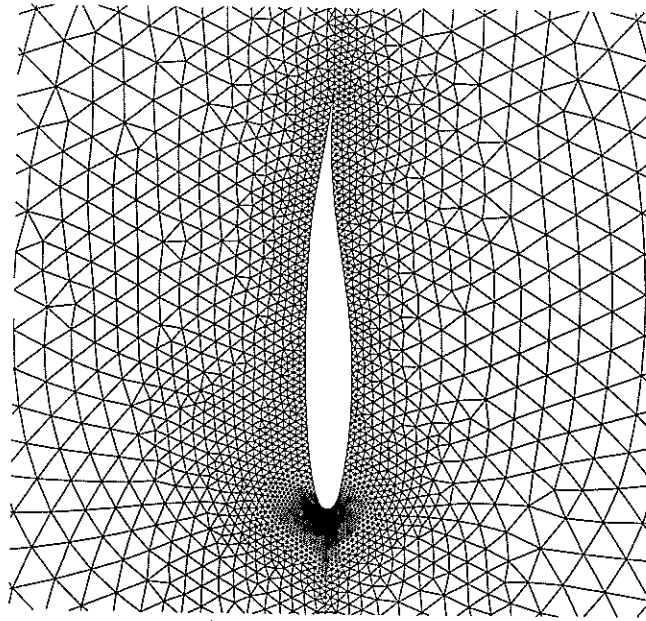


Fig. 22. — Partial view of mesh 3 of the computation domain. Supercritical S airfoil.

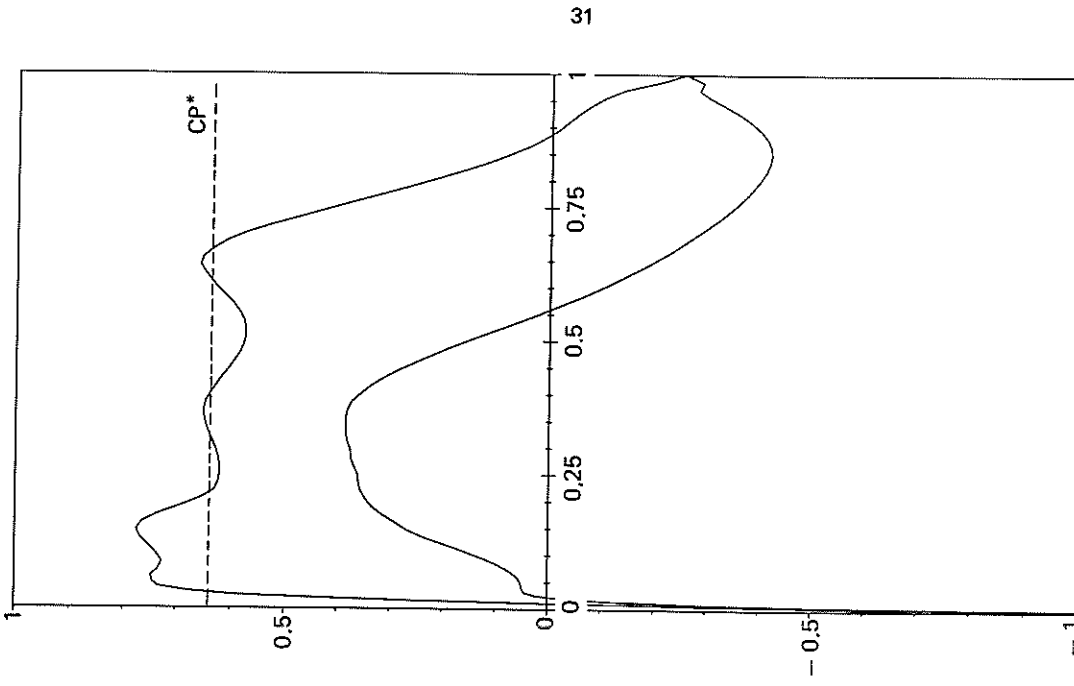


Fig. 23. — Steady pressure coefficient $-C_p$ upper surface and lower surface with mesh 3. Mach 0.735, angle of attack 0.6 degrees. Supercritical S airfoil.

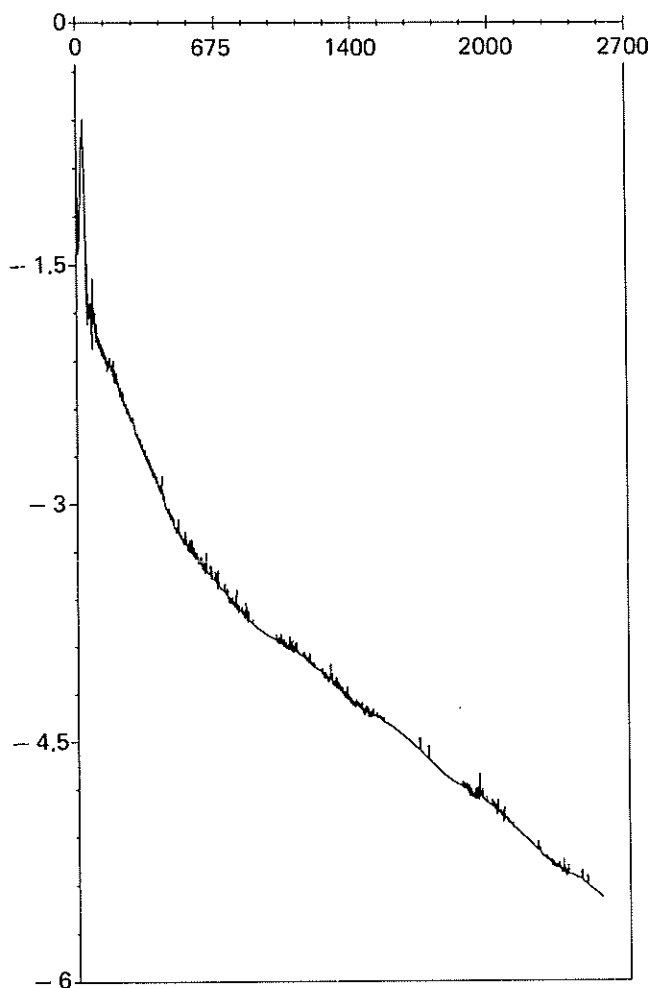


Fig. 24. — Steady convergence, $\log(R2)$, mesh 3. Mach 0.735, angle of attack 0.6 degrees. Supercritical S airfoil.

II.4.2. — UNSTEADY COMPUTATIONS

All the figures represent the results of the harmonic analysis of the unsteady pressure coefficients. The values of harmonics 0, 1 and 2 are given on the ordinate, with the usual sign conventions, and $x_1 = X_1/C \in [0, 1]$ is given on the abscissa. All the figures always show both the upper surface and lower surface (Figs. 27-50). The harmonic analysis is always conducted on the last computation period.

C1INS Results: The reduced frequency is $K=2$ and the computation is made on four periods. Figures 25 and 26 show the Lissajous figures for the lift and

moment. Figures 27-32 are relative to harmonics 0, 1 and 2 of the unsteady pressure coefficient.

C2INS Result: Two reduced frequencies are treated.

A. Reduced frequency $K=0.25$. The analysis was made on three periods and the results are given in Figures 33-39.

B. Reduced frequency $K=2$. The analysis was made on four periods and the results are given in Figures 40-45.

Table IV gives a comparison of the overall values for harmonic 1, with the potential 2D small transonic perturbation code in ADI scheme. The differences are mainly due to the fact that the potential small transonic perturbation code does not include all the time terms in the boundary conditions, contrary to the present formulation which does [52].

C3INS Results: The reduced frequency is $K=0.25$ and the analysis was conducted on three periods starting from the steady solution C6S constructed on mesh 2. The results of the harmonic analysis are illustrated in Figures 46-50.

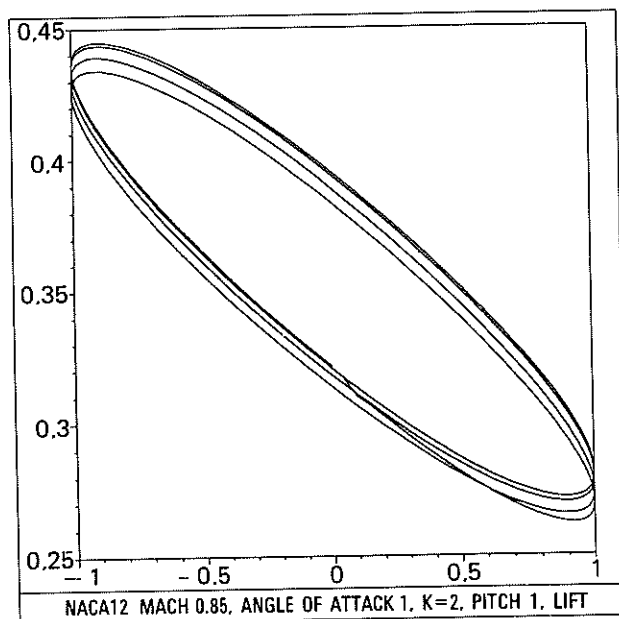


Fig. 25. — Lift Lissajous figure. Movement: forward quarter pitch, amplitude 1 degree, reduced frequency $K=2$.

TABLE IV
Comparisons of the global coefficients on harmonic 1.

| | | Results for harmonic 1 | | Potential small transonic perturbation code - harmonic 1 | |
|----------|--------|------------------------|-------|--|-------|
| | | Modulus | Phase | Modulus | Phase |
| $K=0,25$ | Lift | 5.50 | 152 | 6.68 | 165 |
| | Moment | 0.69 | -167 | 0.59 | -157 |
| $K=2$ | Lift | 5.36 | -159 | 4.61 | -164 |
| | Moment | 1.99 | -131 | 1.82 | -142 |

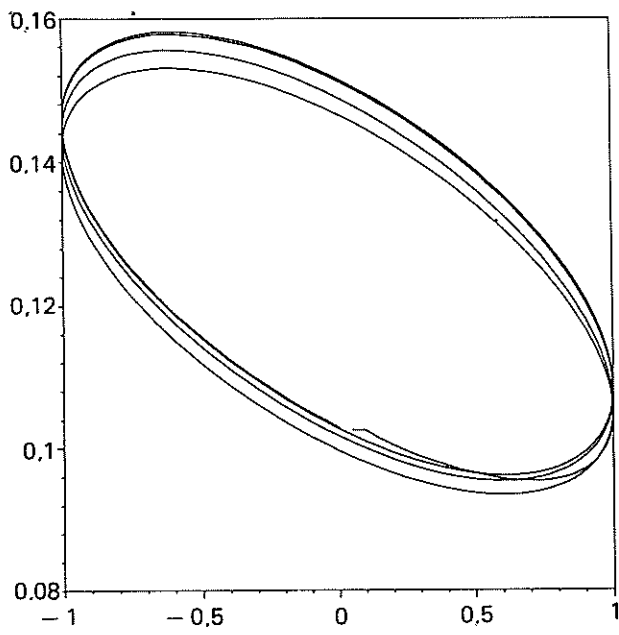


Fig. 26. — Lissajous figure for forward quarter moment.
Movement: forward quarter pitch, amplitude 1 degree,
reduced frequency $K=2$.

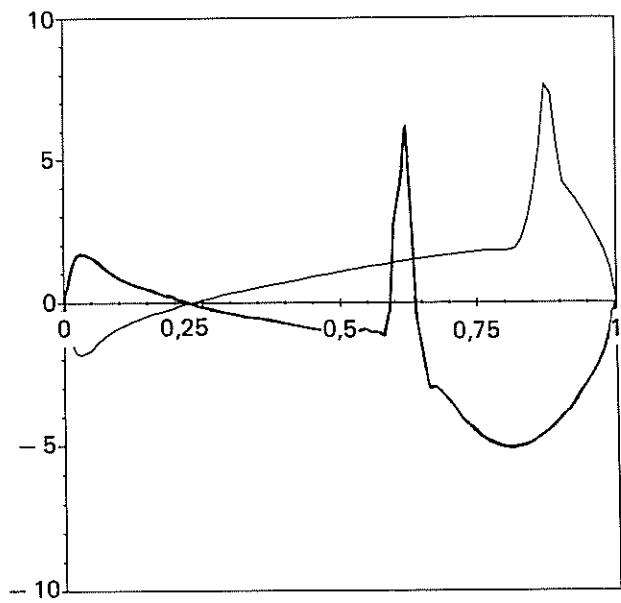


Fig. 29. — Harmonic 1, imaginary part.
Unsteady pressure coefficient.
— Lower surface, — Upper surface.

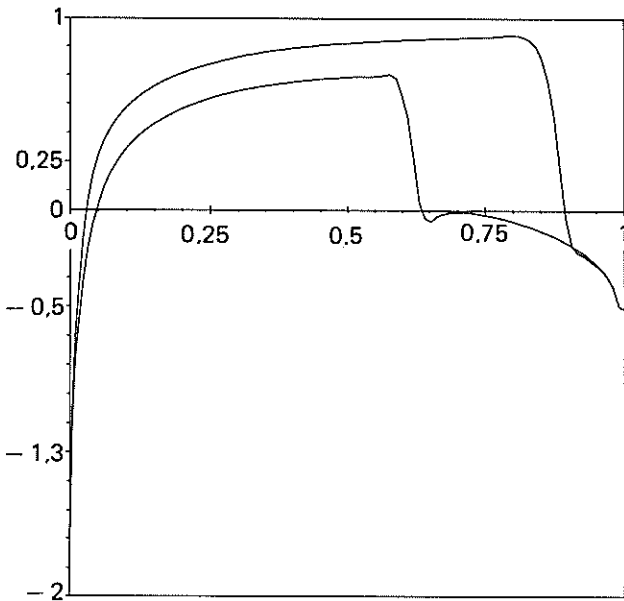


Fig. 27. — Harmonic 0.
Unsteady pressure coefficient on upper surface
and lower surface.

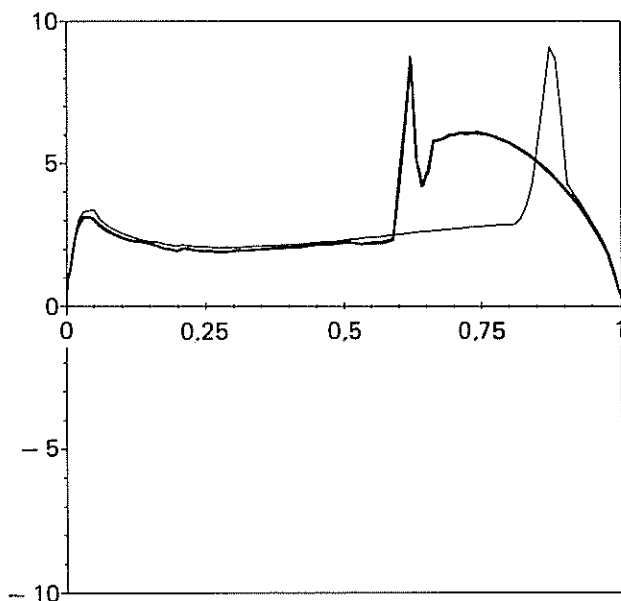


Fig. 30. — Harmonic 1, modulus.
Unsteady pressure coefficient.
— Lower surface, — Upper surface.

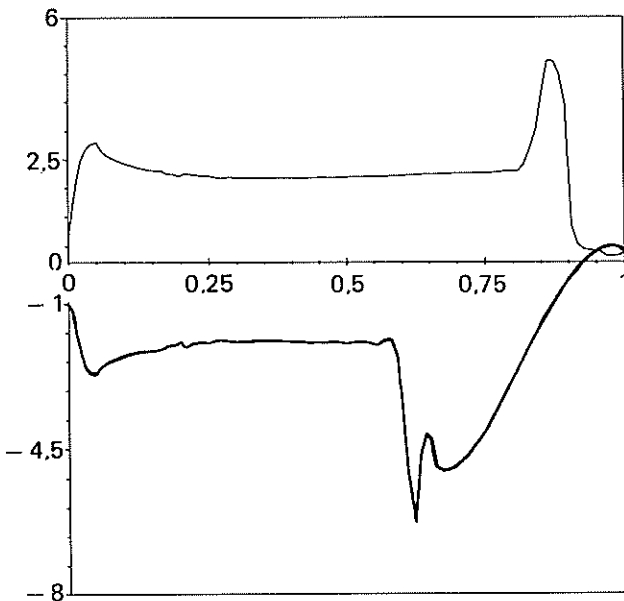


Fig. 28. — Harmonic 1, real part.
Unsteady pressure coefficient.
— Lower surface, — Upper surface.

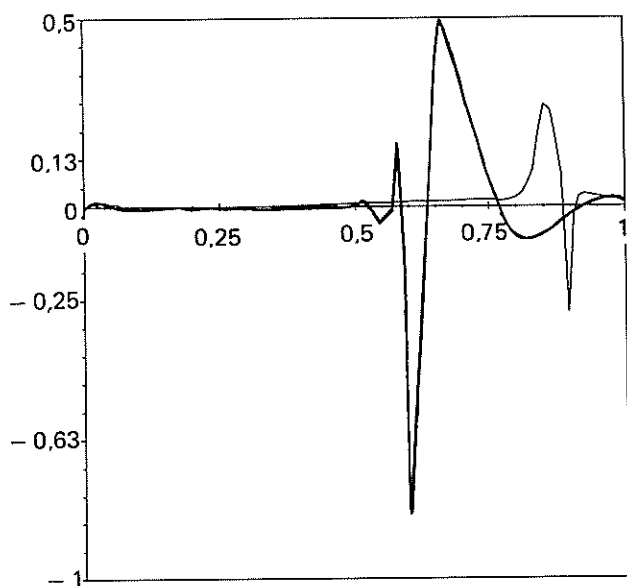


Fig. 31. — Harmonic 2, real part.
Unsteady pressure coefficient.
— Lower surface, — Upper surface.

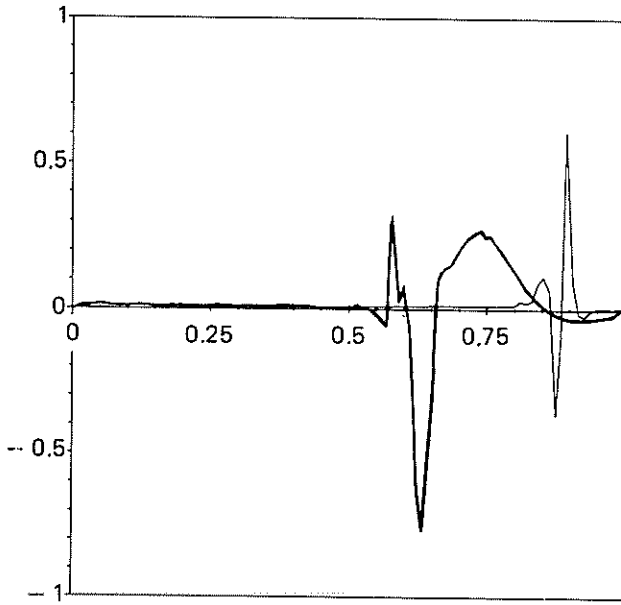


Fig. 32. — Harmonic 2, imaginary part. Unsteady pressure coefficient. — Lower surface, - - - Upper surface.

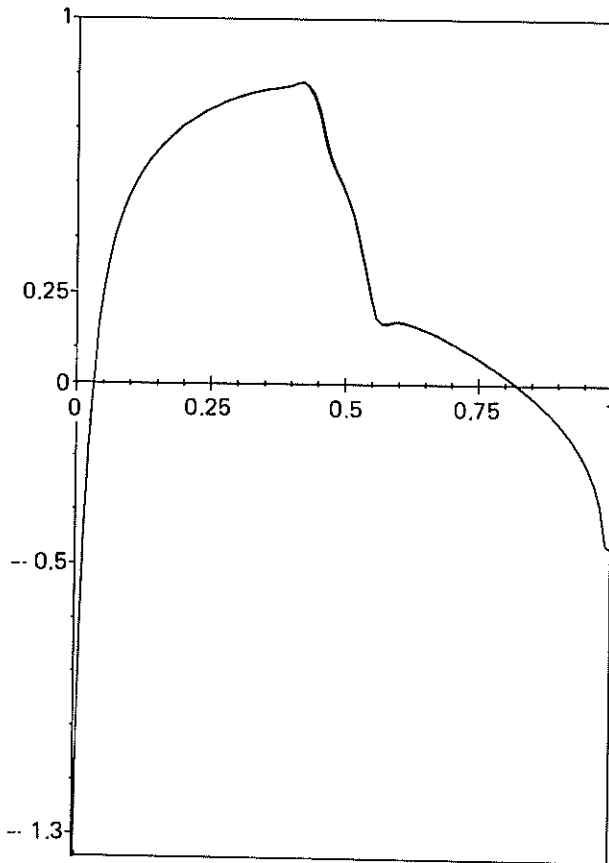


Fig. 33. — Harmonic 0. NACA12 airfoil, Mach 0.80, steady angle of attack 0 degrees. Movement: forward quarter pitch, amplitude 1 degree, reduced frequency $K=0.25$. Unsteady pressure coefficient on upper surface and lower surface.

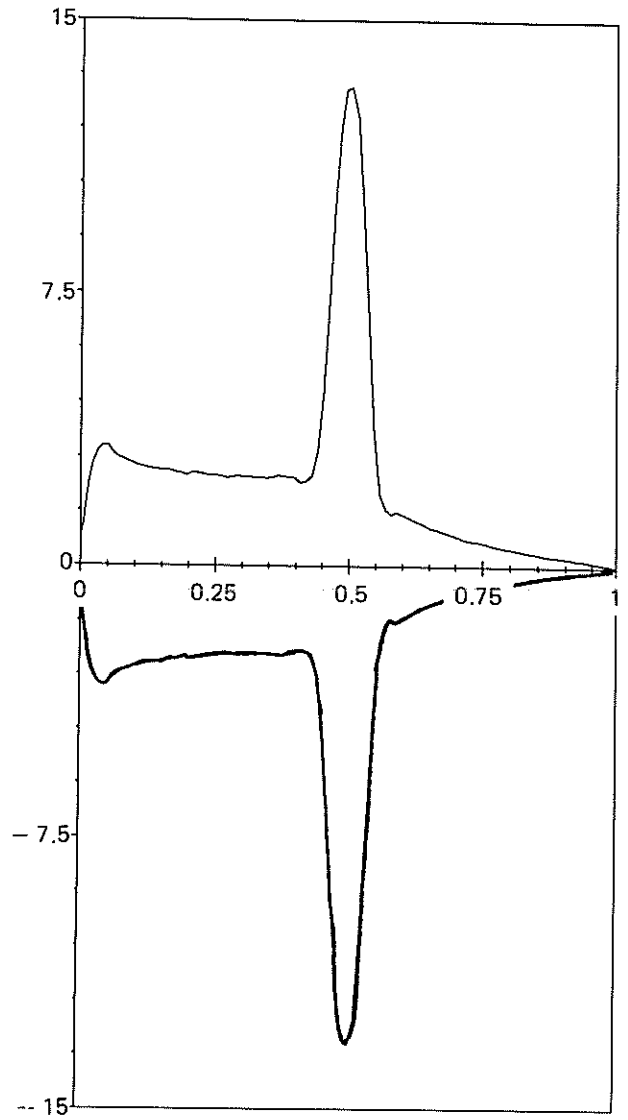


Fig. 34. — Harmonic 1, real part. NACA12 airfoil, Mach 0.80, steady angle of attack 0 degrees. Movement: forward quarter pitch, amplitude 1 degree, reduced frequency $K=0.25$. Unsteady pressure coefficient. — Lower surface, - - - Upper surface.

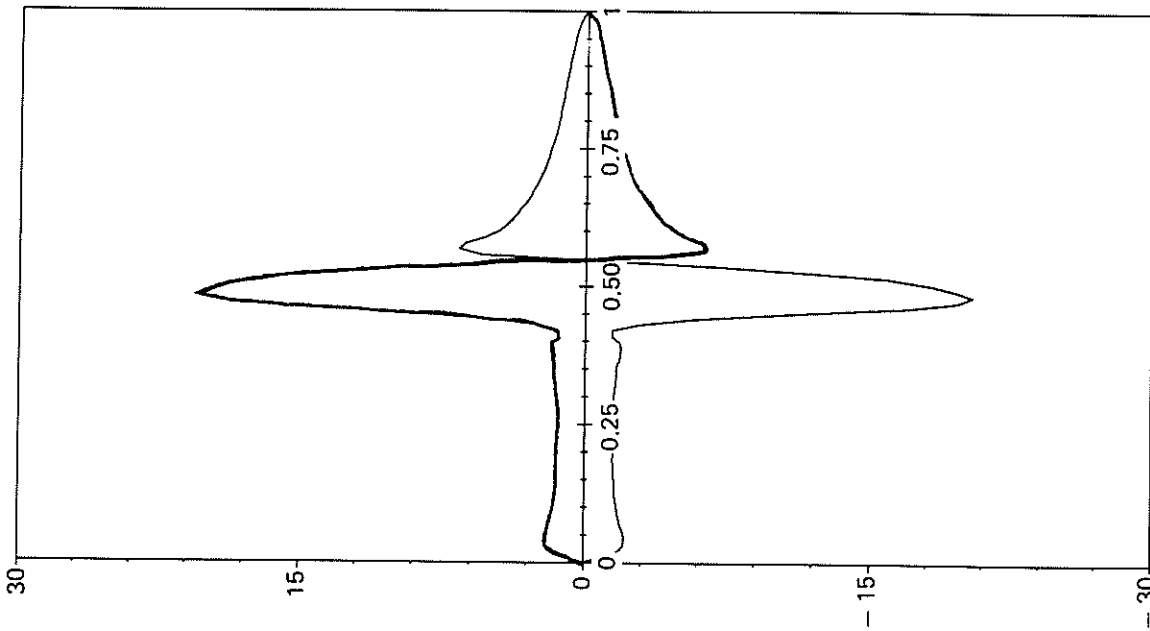


Fig. 35. — Harmonic 1, imaginary part. NACA12 airfoil, Mach 0.80, steady angle of attack 0 degrees. Movement: forward quarter pitch, amplitude 1 degree, reduced frequency $K=0.25$. Unsteady pressure coefficient. — Upper surface.

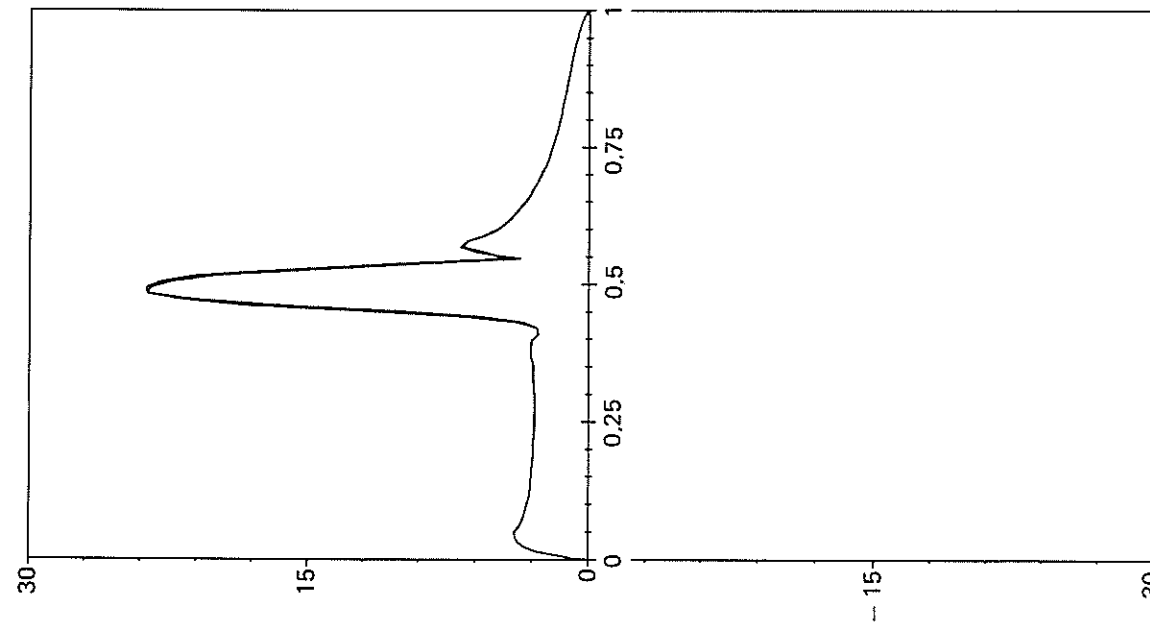


Fig. 36. — Harmonic 1, modulus. NACA12 airfoil, Mach 0.80, steady angle of attack 0 degrees. Movement: forward quarter pitch, amplitude 1 degree, reduced frequency $K=0.25$. Unsteady pressure coefficient on upper surface and lower surface.

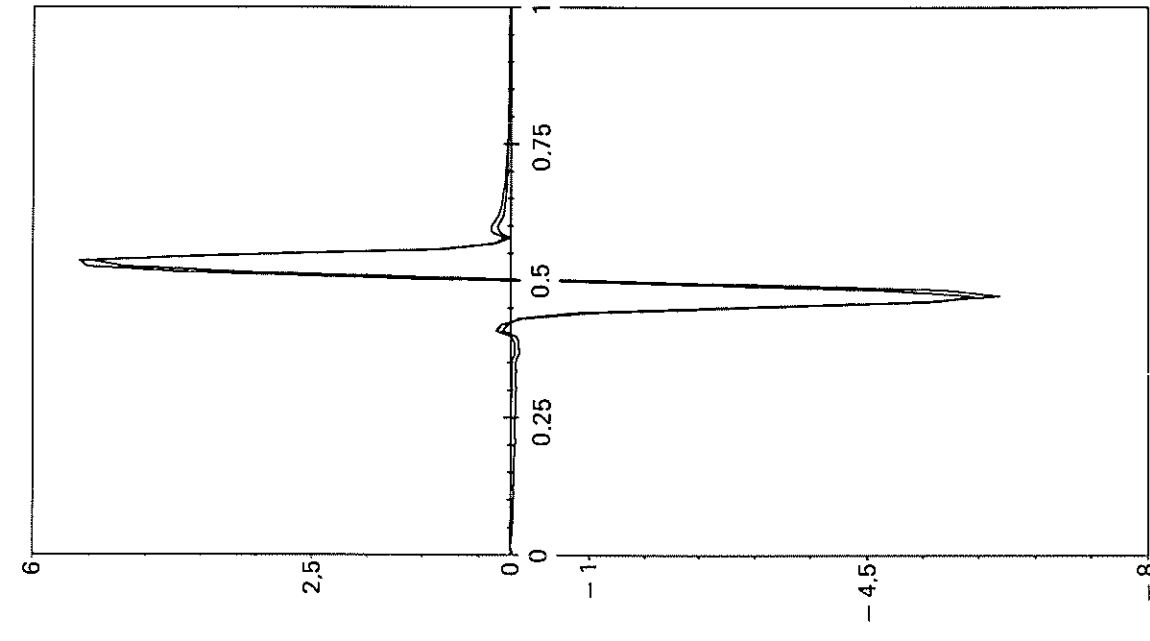


Fig. 37. — Harmonic 2, real part. NACA12 airfoil, Mach 0.80, steady angle of attack 0 degrees. Movement: forward quarter pitch, amplitude 1 degree, reduced frequency $K=0.25$. Unsteady pressure coefficient on upper surface and lower surface.

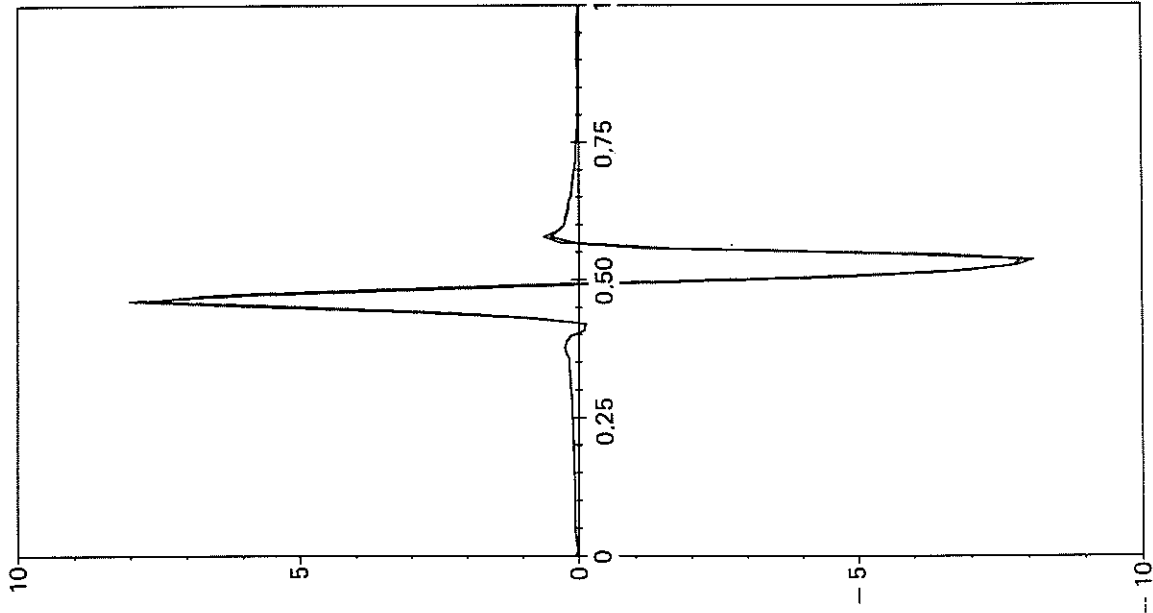


Fig. 38. — Harmonic 2, imaginary part. NACA12 airfoil, Mach 0.80, steady angle of attack 0 degrees. Movement: forward quarter pitch, amplitude 1 degree, reduced frequency $K=0.25$. Unsteady pressure coefficient on upper surface and lower surface.

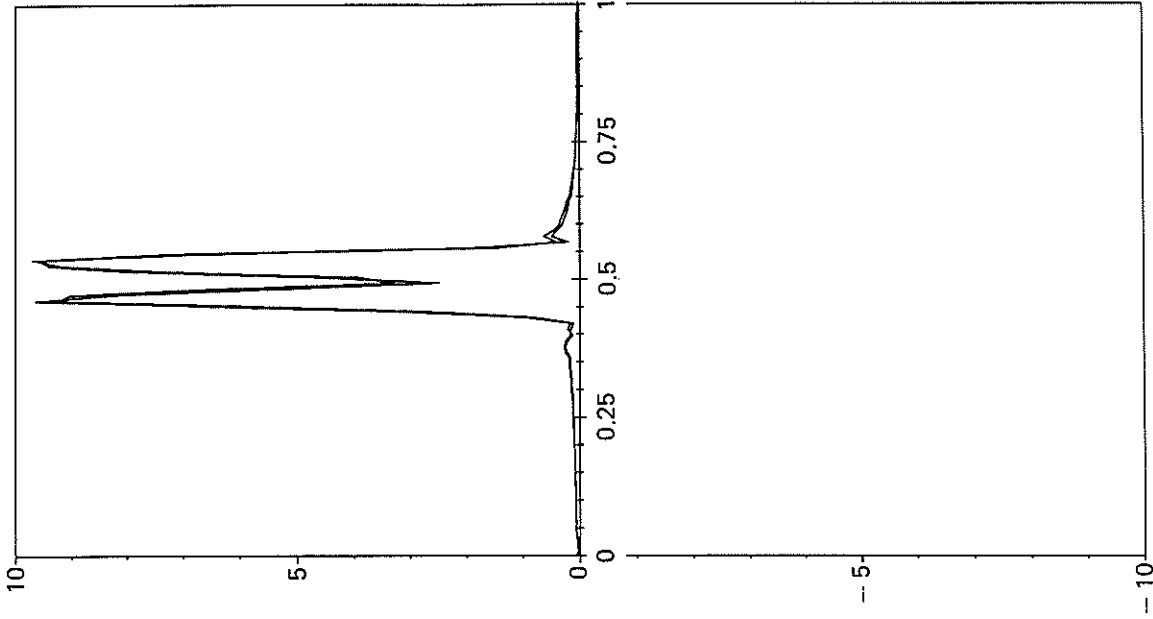


Fig. 39. — Harmonic 2, modulus. NACA12 airfoil, Mach 0.80, steady angle of attack 0 degrees. Movement: forward quarter pitch, amplitude 1 degree, reduced frequency $K=0.25$. Unsteady pressure coefficient on upper surface and lower surface.

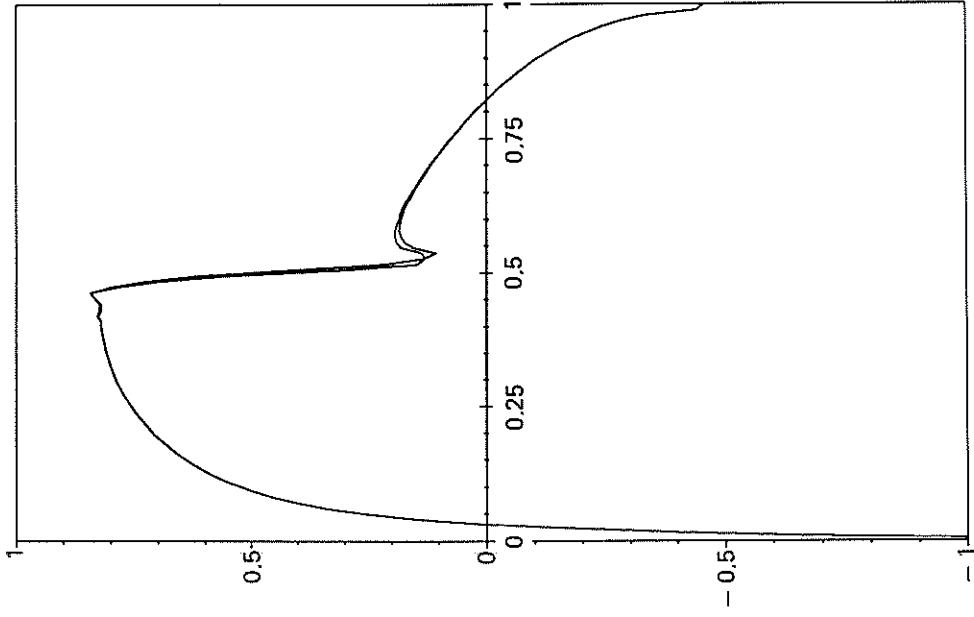


Fig. 40. — Harmonic 0. NACA12 airfoil, Mach 0.80, steady angle of attack 0 degrees. Movement: forward quarter pitch, amplitude 1 degree, reduced frequency $K=2$. Unsteady pressure coefficient on upper surface and lower surface.

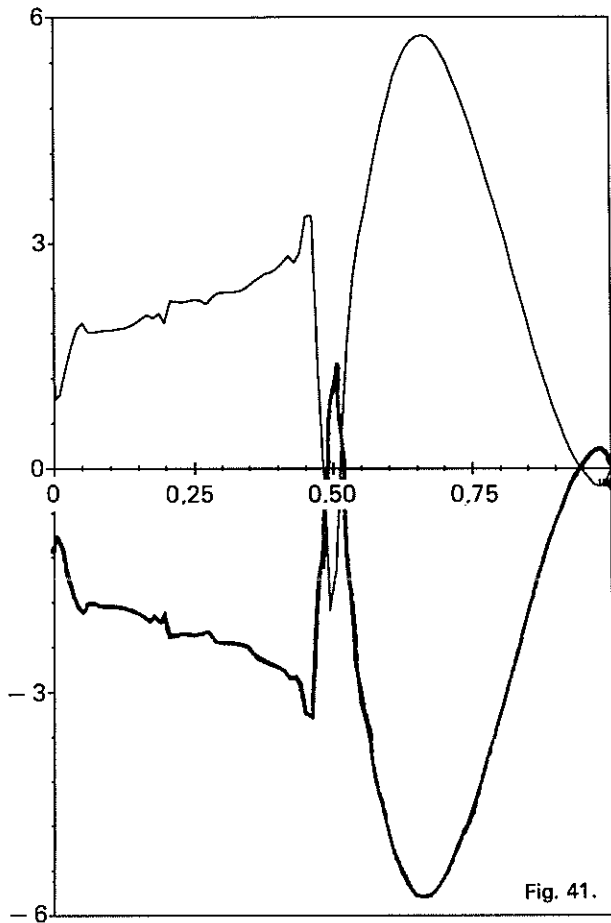


Fig. 41.

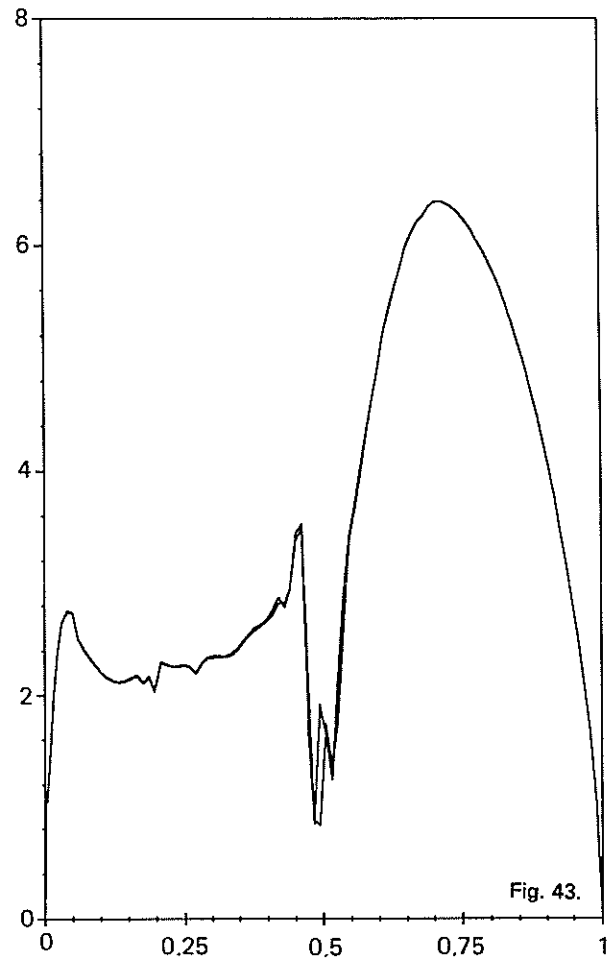


Fig. 43.

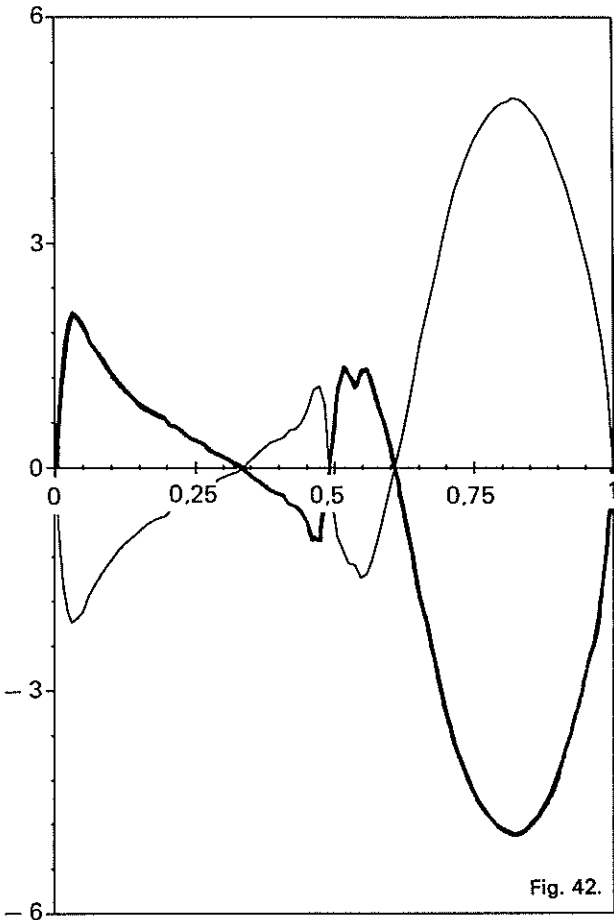


Fig. 42.

Fig. 41. — Harmonic 1, real part. NACA12 airfoil, Mach 0.80, steady angle of attack 0 degrees. Movement: forward quarter pitch, amplitude 1 degree, reduced frequency $K=2$. Unsteady pressure coefficient. — Lower surface, — Upper surface.

Fig. 42. — Harmonic 1, imaginary part. NACA12 airfoil, Mach 0.80, steady angle of attack 0 degrees. Movement: forward quarter pitch, amplitude 1 degree, reduced frequency $K=2$. Unsteady pressure coefficient. — Lower surface, — Upper surface.

Fig. 43. — Harmonic 1 modulus. NACA12 airfoil, Mach 0.80, steady angle of attack 0 degrees. Movement: forward quarter pitch, amplitude 1 degree, reduced frequency $K=2$. Unsteady pressure coefficient on upper surface and lower surface.

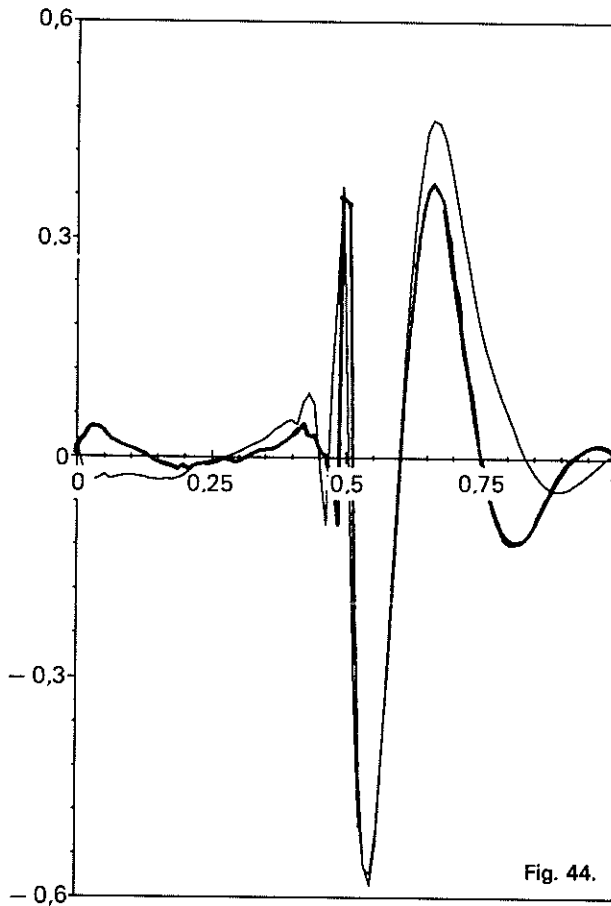


Fig. 44.

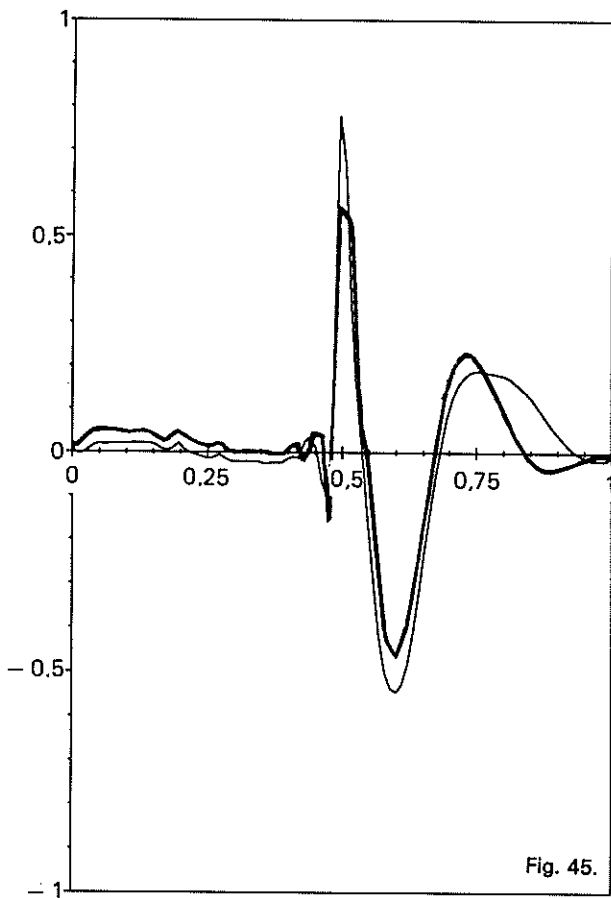


Fig. 45.

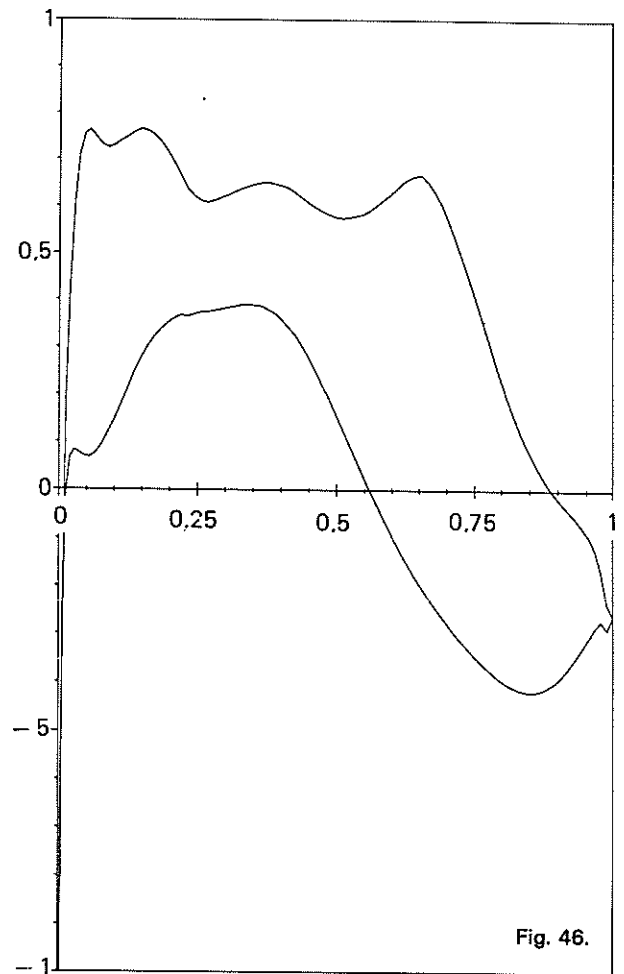


Fig. 46.

Fig. 44. — Harmonic 2, real part. NACA12 airfoil, Mach 0.80, steady angle of attack 0 degrees. Movement: forward quarter pitch, amplitude 1 degree, reduced frequency $K=2$. Unsteady pressure coefficient. — Lower surface, — Upper surface.

Fig. 45. — Harmonic 2, imaginary part. NACA12 airfoil, Mach 0.80, steady angle of attack 0 degrees. Movement: forward quarter pitch, amplitude 1 degree, reduced frequency $K=2$. Unsteady pressure coefficient. — Lower surface, — Upper surface.

Fig. 46. — Harmonic 0. S airfoil, Mach 0.735, steady angle of attack 0.6 degrees. Movement: forward quarter pitch, amplitude 1 degree, reduced frequency $K=0.25$. Unsteady pressure coefficient on upper surface and lower surface.

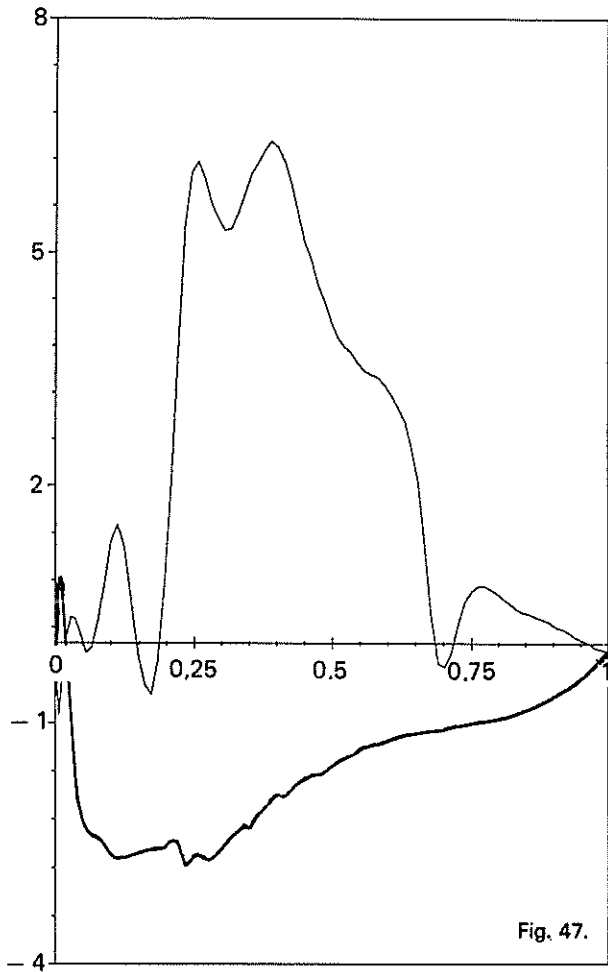


Fig. 47.

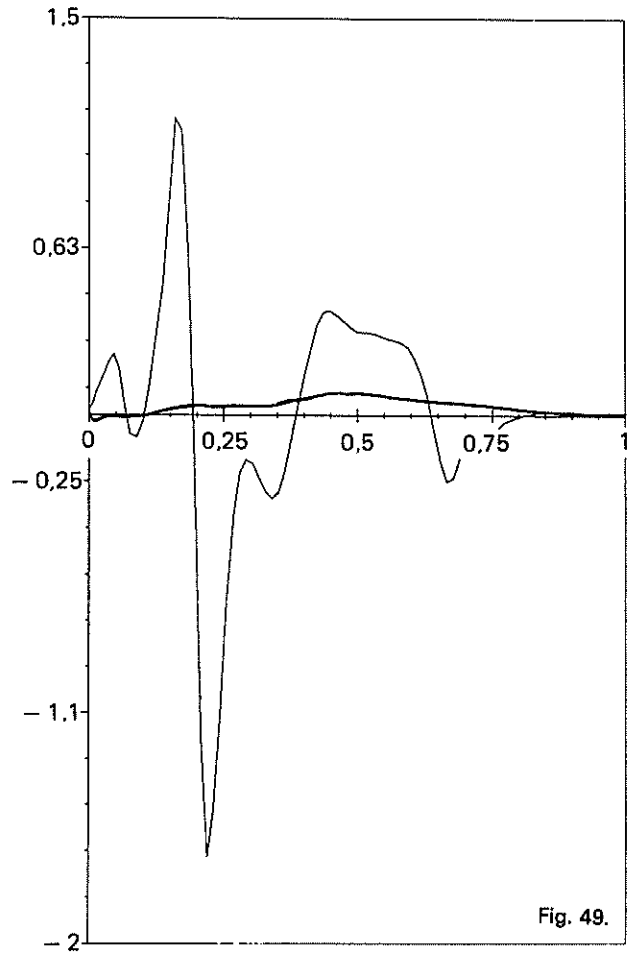


Fig. 49.

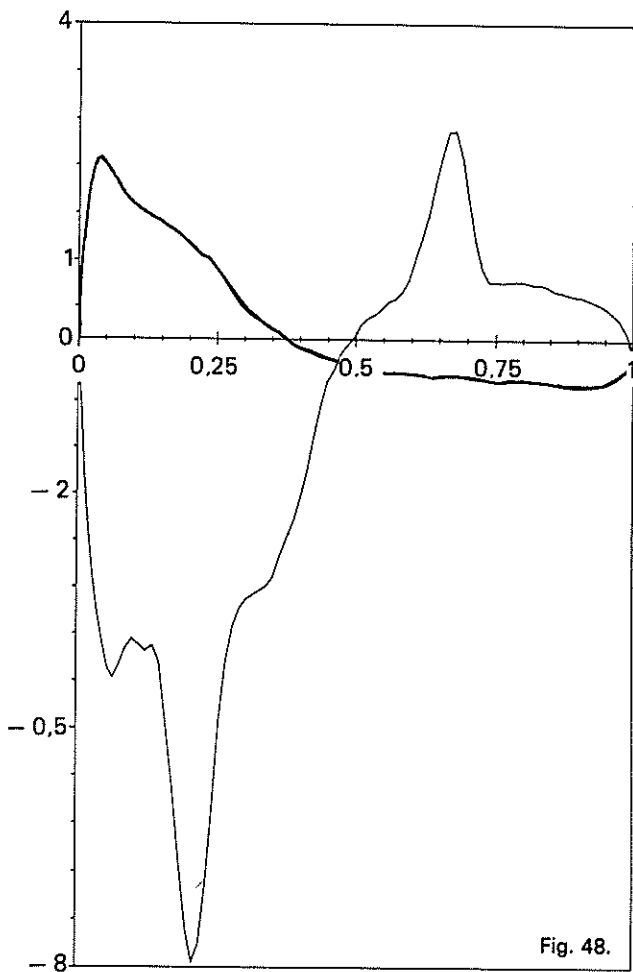


Fig. 48.

Fig. 47. — Harmonic 1, real part. *S* airfoil, Mach 0.735, steady angle of attack 0.6 degrees. Movement: forward quarter pitch, amplitude 1 degree, reduced frequency $K=0.25$. Unsteady pressure coefficient. — Lower surface, - - - Upper surface.

Fig. 48. — Harmonic 1, imaginary part. *S* airfoil, Mach 0.735, steady angle of attack 0.6 degrees. Movement: forward quarter pitch, amplitude 1 degree, reduced frequency $K=0.25$. Unsteady pressure coefficient. — Lower surface, - - - Upper surface.

Fig. 49. — Harmonic 2, real part. *S* airfoil, Mach 0.735, steady angle of attack 0.6 degrees. Movement: forward quarter pitch, amplitude 1 degree, reduced frequency $K=0.25$. Unsteady pressure coefficient. — Lower surface, - - - Upper surface.

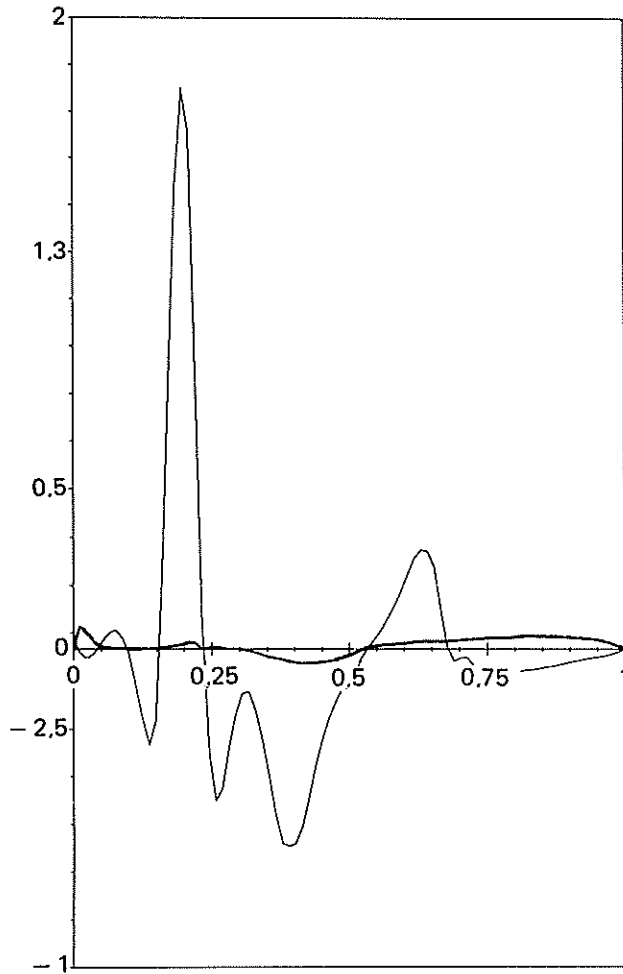


Fig. 50. — Harmonic 2, imaginary part. *S* airfoil, Mach 0.735, steady angle of attack 0.6 degrees. Movement: forward quarter pitch, amplitude 1 degree, reduced frequency $K=0.25$. Unsteady pressure coefficient. — Lower surface, - Upper surface.

II.5. — COMPUTATION TIMES

The CPU times below correspond to the Cray XMP18 serial 332.

II.5.1. — MEAN TIME PER CELL AND PER TIME STEP

For the code developed, the mean time, which is identical for the steady and unsteady cases, is 2.5×10^{-5} seconds per time step and per cell. It should be stressed that the method supports relatively large time steps without deterioration.

II.5.2. — EXAMPLE OF THE COST OF CONSTRUCTING THE SOLUTION FOR THE SUPERCRITICAL *S* AIRFOIL

Steady solution: This solution corresponds to case C6S with mesh 2. Table V gives the CPU time in seconds according to the convergence level.

TABLE V
CPU time for the supercritical *S* airfoil.

| | | | |
|----------------------|--------|--------|--------|
| Number of time steps | 2560 | 1280 | 768 |
| CPU time in seconds | 424 | 216 | 138 |
| Lift | 0.4686 | 0.4705 | 0.4669 |
| Moment | 0.1277 | 0.1270 | 0.1272 |
| log (R2) | -5.51 | -4.11 | -3.60 |

Unsteady solution: This solution corresponds to case C3INS with $K=0.25$. For this reduced frequency, the three periods represent 3072 time steps and the unsteady solution is obtained in 400 seconds. For a reduced frequency $K=1$, the CPU time would be 100 seconds.

II.6. — CONCLUSIONS

The numerical method for solving the finite element type conservative hyperbolic equations described in Part I is used for 2D small transonic perturbations. A 2D code was developed. It was validated for the steady and unsteady case within the limits of approximation of the small transonic perturbations, for the transonic and low supersonic domains. This validation was achieved by comparing the results with reference solutions constructed with the Euler equations for the steady case. The method is robust with respect to the mesh and the choice of the time step. The use of unstructured meshes allows enrichment of the interesting regions of the computation domain to be optimized for a fixed number of finite elements and the mesh to be easily generated for complex geometries at a negligible numerical cost. The computation times remain reasonable, considering that we are working on unstructured meshes, allowing us to consider developing a transonic unsteady 3D code using unstructured meshes.

Manuscript submitted on June 28, 1988.

REFERENCES

- [1] BORREL M., COUAILLIER V., LERAT A., MONTAGNE J. L., SIDES J. and VEUILLOT J. P. — *Comparaison et validation de méthodes de résolution des équations d'Euler*, 23^e colloque d'aérodynamique appliquée, Aussois, (1986).
- [2] FRANCA L. P., HARAI I., HUGHES T. J. R. *et al.* — *Calculation of two dimensional compressible Euler flows with a new Petrov-Galerkin finite element method*, GAMM Workshop, (1986).
- [3] MULAK P., COUSTON M. and ANGELINI J. J. — *Extension of the transonic perturbation approach to three dimensional problems*. International symposium on aeroelasticity, Nuremberg, (1981).

